REPORT DOCUMENTATION PAGE

Form Approved OMB NO. 0704-0188

1. REPORT DATE (DD-MM-YYYY)	2. REPORT TYPE	3. DATES COVERED (From - To)
31-08-2022	Thesis or Dissertation	-

4. TITLE AND SUBTITLE
The Effects of PEGylated Metal-Organic Frameworks for pH-Sensitive Drug Delivery

5a. CONTRACT NUMBER
W911NF-19-1-0001

5b. GRANT NUMBER

5c. PROGRAM ELEMENT NUMBER
106012

6. AUTHORS
Suki Liang

5d. PROJECT NUMBER

5e. TASK NUMBER

5f. WORK UNIT NUMBER

7. PERFORMING ORGANIZATION NAMES AND ADDRESSES
California State University - Los Angeles
5151 State University Drive, GE 314

Los Angeles, CA 90032 -4226

8. PERFORMING ORGANIZATION REPORT NUMBER

9. SPONSORING/MONITORING AGENCY NAME(S) AND ADDRESS (ES)
U.S. Army Research Office
P.O. Box 12211
Research Triangle Park, NC 27709-2211

10. SPONSOR/MONITOR'S ACRONYM(S)
ARO

11. SPONSOR/MONITOR'S REPORT NUMBER(S)
72481-SM-REP.11

12. DISTRIBUTION AVAILIBILITY STATEMENT
Approved for public release; distribution is unlimited

13. SUPPLEMENTARY NOTES
The views, opinions and/or findings contained in this report are those of the author(s) and should not contrued as an official Department of the Army position, policy or decision, unless so designated by other documentation.

14. ABSTRACT

15. SUBJECT TERMS

16. SECURITY CLASSIFICATION OF:			17. LIMITATION OF ABSTRACT	15. NUMBER OF PAGES	19a. NAME OF RESPONSIBLE PERSON
a. REPORT	b. ABSTRACT	c. THIS PAGE			Yangyang Liu
UU	UU	UU	UU		19b. TELEPHONE NUMBER 323-343-2323

REPORT DOCUMENTATION PAGE (SF298)
(Continuation Sheet)

Continuation for Block 13

Proposal/Report Number: 72481.11-SM-REP

Report Title: The Effects of PEGylated Metal-Organic Frameworks for pH-Sensitive Drug Delivery
Report Type: Ph.D. Dissertation

Publication Type: Thesis or Dissertation
Institution: California State University, Los Angeles
Date Received: 31-Aug-2022 Completion Date: 5/19/22 7:03AM
Title: The Effects of PEGylated Metal-Organic Frameworks for pH-Sensitive Drug Delivery
Authors: Suki Liang
Acknowledged Federal Support: **Y**

THE EFFECTS OF PEGYLATED METAL-ORGANIC FRAMEWORKS FOR PH-RESPONSIVE DRUG DELIVERY

A Thesis

Presented to

Department of Mechanical Engineering

California State University, Los Angeles

In Partial Fulfillment

of the Requirements for the Degree

Master of Science

in

Materials Science and Engineering

By

Suki Shiqi Liang

May 2022

The thesis of Suki Shiqi Liang is approved.

Dr. Yangyang Liu, Committee Chair

Dr. Yong Ba, Committee Member

Dr. Oscar Bernal, Committee Member

Dr. Travis Hu, Department Chair

California State University, Los Angeles

May 2022

ABSTRACT

The Effects of PEGylated Metal-Organic Frameworks for pH-responsive Drug Delivery

By

Suki Shiqi Liang

Metal-organic frameworks (MOFs) represent a novel class of hybrid porous nanomaterials that contains high surface modifiable abilities, strengthened drug encapsulation capacities, and improved biocompatibilities for treating resistant cancers. The versatile surface functionality of MOFs enhances the carrier stability to protect the drug from degradation and allows specific distribution of the drug at desired locations. In this work, three zirconium-based MOFs (UiO-66, MOF-808, NU-1000) were incorporated with polyethylene glycol (PEG) chains through click modulation to optimize the drug release efficacy by preventing lysosomal degradation under pH 7.4 and generating a pH-responsive cargo release at pH 5.5, which is the pH that is relatively close to the cancer cell environment. The PEG chains can provide a hydrophilic protective barrier on MOFs to prevent their rapid degradation under pH 7.4 (healthy cell environment). As the pH becomes more acidic, the PEG can depolymerize and the MOF ligands can dissociate to degrade the MOFs to further release the encapsulated drug. This unique design endows the PEGylated MOFs with pH-responsive properties and targeted drug delivery capability. In this study, both uncoated and PEG-coated MOFs with diverse structures were investigated to examine the effects of PEGylation on drug delivery.

ACKNOWLEDGMENTS

I would like to acknowledge and express my sincere gratitude to my thesis advisor, Dr. Liu, who made this work possible. I am grateful for being part of Dr. Liu's group and had the opportunity to participate in my interested research. Dr. Liu's guidance, insightful advice, continuous support, and patience carried me through all stages of the project. Dr. Liu's extensive experience and knowledge in chemistry helped me to complete this research.

I would also like to give special thanks to my committee members, Dr. Yong Ba and Dr. Oscar Bernal for their valuable comments and suggestions which pushed me to sharpen my thinking and complete this work with better understanding.

Lastly, I would like to thank everyone that involved in this work. To Brandon Liu, Willmer Flores, and Alberto Smith, who started the project. Thanks to Nikita Mishra and Becky Huang for helping me to complete this work. Thanks to everyone in the group, it is my pleasure to be part of the group.

This research was partially sponsored by the Army Research Office and was accomplished under Grant Number W911NF-19-1-0001. This research was also supported by Provost's Research Restart Funds (post lab shutdown due to COVID-19) from Cal State LA. Financial support also comes from the College of Natural and Social Sciences for offering a Graduate Research Assistant Fellowship to Suki Liang.

TABLE OF CONTENTS

LIST OF TABLES

Table

LIST OF FIGURES

Figure

CHAPTER 1

Background and Introduction

1.1 Cancers

Cancers are diseases that involve uncontrollably abnormal cell growth with the potential to spread to other body parts and destroy the nearby normal body tissues. Additionally, cancers can become lethal as they disrupt the tissues and stop organs from functioning properly for the survival of the organisms[1]. There are around 37 trillion cells contained in the average normal human body, each with its own structure and function. In order for an organism to grow and maintain its health, normal cells regulate one another's proliferation and only reproduce when instructed to do so.[1] In contrast, mutations in particular genes in cancer cells prevent them from regulating cell growth, and eventually, the uncontrollable cell growth leads to metastasis throughout the body and causes life-threatening complications[2].

Cancer is a leading cause of death worldwide. More than 19 million people are diagnosed with cancer and nearly 10 million people die of cancer annually[3]. In the near future, the World Health Organization has estimated that there will be over 20 million new cancer cases diagnosed and 13 million cancer-related deaths by the year 2030[4]. In spite of that, the mortality rate has decreased in the past 20 years by 27% due to improved cancer treatments and diagnostic devices[5]. Current common treatments for cancer are surgery therapy, radiation therapy, and chemotherapy. Among all these treatments, chemotherapy is considered the safest treatment with promising efficiency in killing cancer cells. Chemotherapy is a type of cancer treatments that involves the use of anticancer drugs to cure cancers.

1.2 Chemotherapy

Chemotherapy can be classified into two main categories: conventional chemotherapy (conventional drug delivery system) and novel chemotherapy (novel drug delivery system). The conventional drug delivery system involves the traditional direct administration of therapeutic drugs including oral, inhalation, topical, or intravenous injection[6]. Although conventional chemotherapy can effectively kill cancer cells, the limitation of lacking specificity for discriminating between normal cells and cancer cells usually induces diverse side effects[7]. Numerous studies have also demonstrated that the conventional drug delivery system has poor bio-accessibility[5], high-dose requirements, and inability to achieve therapeutic concentrations[8], which results in low efficacy under the increased incidence of multiple drug resistance.[5] Therefore, novel drug delivery systems are developed in recent decades to overcome these issues and eliminate all the limitations associated with the conventional drug delivery system.[9]

1.3 Novel Drug Delivery System (NDDS)

Novel drug delivery systems (NDDSs) are enhanced drug delivery systems that use drug carriers to transport the therapeutic agents to the target area. Various NDDSs are being investigated, and multiple drug carriers were developed for drug delivery purposes. Some organic carriers, including liposomes, micelles, and some polymeric nanoparticles, are capable of protecting the encapsulated drug from degradation[10] to increase drug circulation time for sustained release[10-11]. However, the disadvantages of organic NDDs include the low drug loading efficiency and low stability[12]. On the other hand, inorganic carriers such as mesoporous silica composite and some metallic nanoparticles have greater loading capacity due to their well-ordered internal pores and large surface areas

(700-1000 m^2/g)[13]. However, the major concern of using inorganic carriers to transport therapeutic agents is the toxicity of their degraded components.[13-14] Developing an ideal drug carrier remains one of the most challenging tasks for the scientific community. An ideal drug carrier is considered to have the following properties: enhanced drug uptake, ability to release drug at the targeted area, enhanced stability under circulation, and low cytotoxicity. Herein, a type of hybrid inorganic-organic material called metal-organic frameworks (MOFs) was introduced as a potential candidate for an ideal drug delivery carrier for its unique properties.

1.4 Metal-Organic Frameworks (MOFs)

MOFs are a class of inorganic-organic hybrid porous crystalline materials that form coordination networks of metal clusters and organic linkers (as shown in Figure 1).[15]

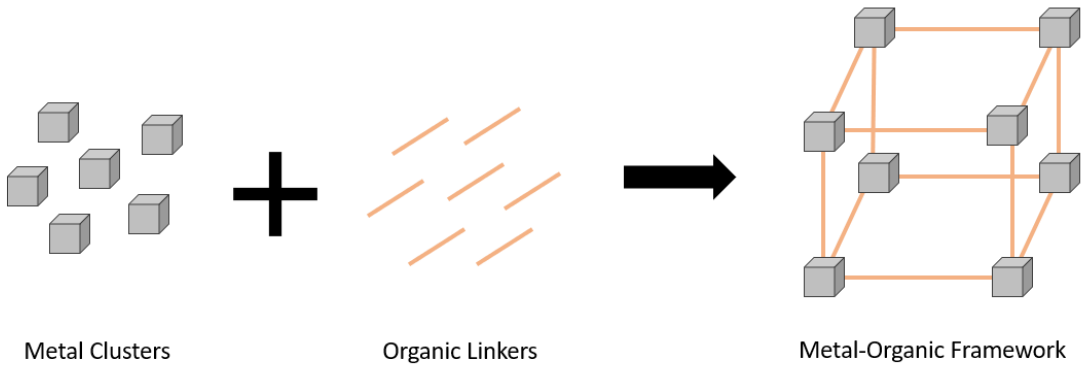

Figure 1. Metal-Organic Framework

The combination of the metal-containing inorganic secondary building units (SBUs)[16] and the organic ligands enabled the high porosity, thermal stability, and mechanical stability of the MOFs through the strong coordinate covalent bonds. Due to their versatile structures, internal porosity[17], high surface area[18], excellent structural stability, and great biocompatibility, MOFs have been investigated increasingly in diverse

fields for their potential applications such as gas storage[19], gas separation[20], catalysis[21], and drug delivery[7].

1.5 MOFs as Drug Delivery Carriers

More importantly, MOFs can be considered ideal potential drug delivery carriers because of their tailorable structures and easy surface modifiable ability.[22] These characteristics of MOFs endow them with the capability to address the limitations of the other drug delivery systems.

In particular, the adjustable structures of MOFs enable their ability to transport sufficient amounts of therapeutic agents in order to optimize the encapsulation efficacy. Specifically, the adjustment of MOFs can be achieved by incorporating different organic linkers. For instance, Abánades Lázaro *et al.* reported the use of the zirconium terephthalate MOF UiO-66 as a delivery vehicle for the therapeutic agent calcein and a drug loading efficiency of around 16 wt% was observed.[7] Meanwhile, Zhao *et al*. employed another zirconium-based MOF NU-1000 as delivery cargo for the anticancer drug Doxorubicin hydrochloride and about 35 wt% of the drug was loaded into the NU-1000.[23] The similarity of UiO-66 and NU-1000 is that both of them are zirconium-based MOFs. However, the organic linkers for UiO-66 and NU-1000 are the terephthalic acid and 1,3,6,8-tetrakis(*p*-benzoic-acid)pyrene (H_4TBAP_y), respectively. The pore sizes of UiO-66 and NU-1000, as a result, are 10.2 Å and 30.0 Å, respectively.[24] The structures of the coordination networks are strongly influenced by the combinations of metal clusters and organic linkers. Different metal-linker combinations could potentially lead to varying drug loading capacities.

Additionally, to further enhance the stability of MOFs as delivery carriers to prolong circulation lifetimes, surface modification of polyethylene glycol (PEG) chains on MOFs through mild bioconjugate reactions has shown promising protective ability.[7] Abánades Lázaro *et al*. reported the PEG chains coated UiO-66 with the therapeutic agent calcein encapsulated released around 40% of calcein under pH 7.4 while the naked calcein loaded UiO-66 released more than 80% of calcein under pH 7.4.[7] The PEG chains coating was observed to be able to protect the drug from being rapidly released in the circulation (pH7.4). Hence, PEG chain incorporation is essential for improving the stability and increasing the circulation time of the MOFs.

1.6 Polyethylene glycol (PEG) coating

PEG is a hydrophilic linear polyether compound derived from polymerizing monomers of ethylene oxide with hydroxyl groups at both ends, which allow PEG to induce easy conjugation with various functional groups.[28] Therefore, surface functionalization on drug delivery carriers with PEG coating, or "PEGylation", is widely utilized in drug delivery to improve the biophysical and chemical properties of carriers. Abuchowski *et al.* reported the first PEG covalently attachment to liver catalase proteins for drug delivery in 1977 and observed that the PEGylation could increase the circulation time with no immune response.[25] Beginning in 1990, the FDA successively approved PEGylated therapeutic products to treat diseases.[26] The long history studies of PEG have proven that PEGylation coating is capable of protecting the drug delivery carriers such as MOFs from opsonization and phagocytosis.[27]

Transporting therapeutic agents by drug delivery carriers to the targeting tumor sites has been challenging due to the mononuclear phagocytic system (MPS). The MPS is

responsible for the clearance of foreign particles through opsonization.[28] Foreign particles that enter the bloodstream are likely to be recognized by opsonins as pathogens during circulation. Opsonins are serum proteins that serve as tags to label particles that are needed to be phagocytosed by adsorbing onto the surface of the foreign particles.[27] Any opsonin-tagged foreign particles will then undergo phagocytosis and be removed by the MPS. PEG coating on delivery carriers creates a hydrophilic protective barrier that is against opsonins binding by resembling the cellular membranes.[7, 29] Hence, surface modification on MOFs with PEG chains is desirable to minimize opsonins attachment[30], inhibit removal by the MPS[30], avoid rapid elimination by phagocytes[28], and prolong circulation time for MOFs to reach the targeted tumor site.

1.7 Design PEGylated MOFs for Drug Delivery

In this project, zirconium-based MOFs (Zr-MOFs) were selected due to their excellent biocompatibility for low cytotoxicity and great stability for enhanced drug uptake. In addition, the chemical stability of Zr-MOFs can be influenced by the other ions in a certain operating environment. For instance, the presence of phosphate ions in phosphate-buffered saline (PBS) are more likely to attack the Zr metal clusters and replace the ligands, leading to MOFs degradation.[31] This property of Zr-MOFs allows them to decompose and release the encapsulated drug in an acidic condition. Moreover, post-synthetic modification of PEG conjugation on Zr-MOFs facilitates the pH-responsive release of cargo by preventing opsonizing plasma proteins[32] and prolonging the circulation time of the carriers for them to reach the desired tumor sites.

Herein, a functionalized modulator, 4-aminomethylbenzoic acid (4-AMBA) was selected to incorporate onto the Zr-MOFs using solvent-assisted ligand incorporation

(SALI). Following the surface functionalizing of 4-AMBA, PEG chains were modified onto Zr-MOFs by the copper(I)-catalyzed azide-alkyne cycloaddition (CuAAC).[7]

Calcein was used in this study as a model drug because of its structural similarities to a widely known anticancer drug, doxorubicin.[33] The loading and release efficiency of calcein from the modified Zr-MOFs were analyzed using dialysis bags under pH 7.4 (simulated healthy biological system environment) and pH 5.5 (simulated tumor site environment).

CHAPTER 2

Materials and Characterizations

2.1 Zirconium-based MOFs (UiO-66, MOF-808, NU-1000)

In this project, three zirconium-based MOFs (Zr-MOFs)), UiO-66[34], MOF-808[35], NU-1000[36], were selected due to their excellent biocompatibility, low cytotoxicity, and pH-responsive decomposition ability. As shown in Figure 2, the combinations of different ligands with the zirconium metal cluster generated three MOFs with completely different geometries and pore sizes.

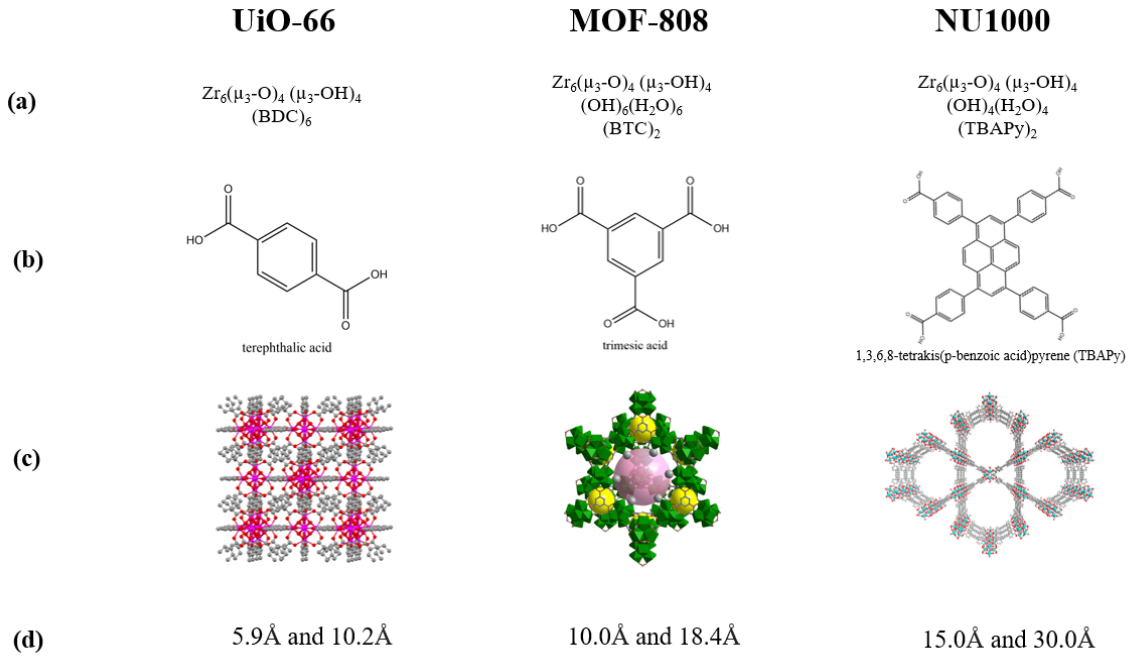

Figure 2. Characteristics of Selected Zr-MOFs: (a) the formulas (b) the ligands (c) the structures (d) the pore sizes of the selected Zr-MOFs

UiO-66 is a Zr-based MOF with terephthalic acid (1,4-benzene dicarboxylic acid) ligand. Previous studies showed that UiO-66 has a its Brunauer-Emmet-Teller (BET) surface area of around 1,187 m^2/g, pore volume of 0.5 cm^3/g, and pore sizes of 5.9 Å and 10.2 Å.[37] Furthermore, UiO-66 was proven as a biocompatible material which yields a

half maximal inhibitory concentration (IC_{50}) of 1.50 ± 0.15 mg/mL toward the HeLa cell line after 24 hours of exposure.[7] MOF-808 is a Zr-based MOF with trimesic acid (1,3,5-benzene tricarboxylic acid) ligand. As reported by a previous study, its BET surface area is around 2,060 m^2/g[38], its pore volume is 0.84 cm^3/g[38], and the pore sizes of MOF-808 are 5.9 Å and 10.2 Å[24]. NU-1000 is a Zr-based MOF with 1,3,6,8-tetrakis(*p*-benzoate)pyrene (TBAPy) ligands. NU-1000 was reported to have a BET surface area of around 2,145 m^2/g, pore volume of 1.46 cm^3/g, and pore sizes of NU-1000 are 15 Å and 30 Å.[39]

UiO-66, MOF-808, and NU-1000 were surface-functionalized with the modulator 4-Amidemethylbenzene acid (4_AMBA) using solvent-assisted ligand incorporation (SALI) for further modification with PEG chains via copper-catalyzed azide–alkyne cycloaddition (CuAAC). Figure 3 shows the modification procedures of Zr-MOFs.

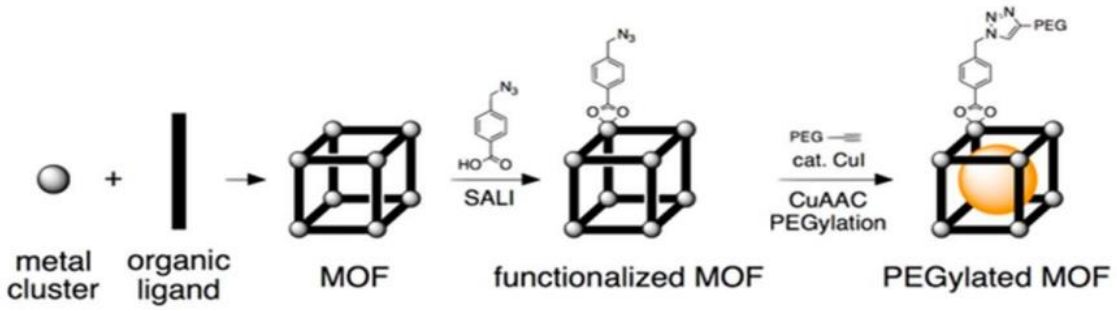

Figure 3. A schematic illustration of the MOF modification process

2.2 Post-synthetic Modification on MOFs with 4_AMBA (MOF-4_AMBA)

Solvent-assisted ligand incorporation (SALI) was adapted to accomplish the incorporation of 4-amidemethylbenzene acid (4_AMBA) as a modulator into the Zr-based MOFs for further modifications such as click chemistry.[40] In this study, MOFs that

were successfully incorporated with 4_AMBA are denoted as UiO-66-4_AMBA, MOF-808-4_AMBA, and NU-1000-4_AMBA respectively.

The Zr_6^{IV} metal nodes-based MOFs were demonstrated by various studies for retaining high thermal and chemical stabilities under high temperatures. The post-synthetic modification on MOFs using SALI induced an acid-base reaction between the carboxylic group of the modulator 4_AMBA and a pair of terminals hydroxylic ligands of the Zr_6 cluster.[40] After SALI, the desired functionalities containing the azide group of 4_AMBA should point outward while the carboxylic group of 4_AMBA is attached to the Zr_6 nodes.[7] The azide functional groups can serve as a platform for further post-synthetic modification.

It is worth noting that the post-synthetic modification of 4_AMBA did not involve any replacement of the organic ligands or any deformation of the MOFs. The crystalline structures of UiO-66-4_AMBA, MOF-808-4_AMBA, and NU-1000-4_AMBA can be confirmed by powder X-ray diffraction (PXRD). In addition, the presence of the azide vibration band of 4_AMBA on modified MOFs can be detected by Fourier transform Infrared spectroscopy (FT-IR) at 2,100 cm^{-1}.

2.3 Post-synthetic Modification on MOFs with PEG550-Propargyl (MOF-PEG)

After the modulator 4_AMBA was successfully incorporated into the Zr-MOFs, resulting in the accessible reactive azide functional group to react with the terminal alkynes of PEG550-Proparyl in a copper-catalyzed reaction called “copper(I)-catalyzed azide-alkyne cycloaddition (CuAAC)”. Jankovič *et al.* reported that the CuAAC reaction could be applied to all types of starting alkyne reagents and organic azide reagents,

forming 1,2,3-triazoles.[41] Hence, CuAAC is also widely used for PEGylation of drug delivery carriers.

In this study, the propargyl-ended PEG was synthesized to react with the azide group of 4_AMBA, obtaining the PEGylate MOFs for increased hydrophilicity, reduced interaction with opsonins proteins, and thus prolonged circulation time in the bloodstream. In this thesis, PEGylated MOFs are denoted as UiO-66-PEG, MOF-808-PEG, and NU-1000-PEG, respectively.

Successful surface PEGylation of MOFs can be confirmed using PXRD and FT-IR. PXRD was used to confirm the crystalline structure of the PEGylated MOFs, and FT-IR spectra were used to verify the incorporation of PEG with the disappearance of the triazole bands.

2.4 Calcein

Calcein has often been employed as a model drug in drug delivery-related studies due to its similar structure to a widely used anticancer drug called Doxorubicin (DOX).[42]

The chemical structures of Calcein and DOX are shown below in Figure 4. The carboxyl groups of calcein endow it with a hydrophilic character. Particularly, the -COOH group on calcein is a strongly hydrophilic group which means that calcein cannot permeate the cell membrane itself, and it requires a drug delivery carrier to cross the membrane to enter the cells.[7] Moreover, calcein is also a fluorescent molecule and can be detected by UV-Vis spectrophotometric (UV-Vis). In our study, calcein was used as a model drug and loaded in the Zr-MOFs, and the release of calcein was monitored using UV-Vis.

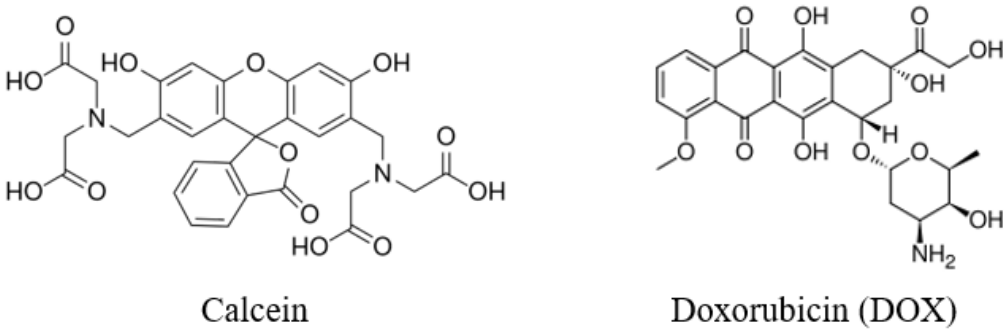

Figure 4. Chemical Structures of Calcein and Doxorubicin

CHAPTER 3

Materials and Methods

3.1 Materials

Zirconyl chloride octahydrate (98%), Zirconium(IV) chloride, Terephthalic acid (BDC), *N*,*N*–dimethylformamide (DMF, 99.8%), Acetone (99.5%), 1,3,5-Benzenetricarboxylic acid (BTC, 98%), Formic acid (98 %), Benzoic acid (99.5%), Trifluoroacetic acid (TFA, 97%), 4-(methoxycarbonyl) phenyl)boronic acid (95%), 1,3,6,8-tetrabromopyrene (98%), Potassium Phosphate tribasic (98%), Tetrakis(triphenylphosphine)palladium(0) (99%), Anhydrous 1,4-Dioxane (99%), Chloroform ($CHCl_3$, 99.8%), Sodium Hydroxide (NaOH, 97%), Tetrahydrofuran (THF, 99.8%), Methanol (MeOH, 99.8%), Hydrochloric acid (HCl), 4-(Bromomethyl) benzoic acid (97%), Sodium azide (NaN_3, 99%)), Sodium Hydride (NaH), Poly(ethylene glycol) methyl ether average M_n 550 (PEG550), Propargyl bromide (97%), Anhydrous tetrahydrofuran (THF, 99.8%), and Calcein were purchased from commercially available sources (Fisher Scientific and Sigma Aldrich) and used without further purification.

3.2 Instrumentation

Powder X-ray Diffraction (PXRD) measurements were recorded on Bruker D2 Phaser (CuKα radiation, λ = 1.5418 Å). Data were collected over the range of 2^o-20^o. Nuclear Magnetic Resonance Spectroscopy (NMR) was recorded on Bruker Avance III 400 MHz spectrometer. UV-Vis Spectroscopy data were recorded using a Shimadzu UV-2600, and analysis was carried out using the software LabSolutions UV-Vis. Fourier transform Infrared spectroscopy (FT-IR) of samples were collected using a PerkinElmer Fourier Transform Infrared Spectrometer, UATR Two, fitted with a Diamond chip.

Analysis was carried out from using the software Spectrum. N_2 adsorption isotherms were carried out at 77 K on gas sorption analyzer ASAP 2020. Samples were degassed according to the protocols under vacuum at 120°C-150°C for 12-15 hours. BET surface areas of MOF samples were calculated from the isotherms using ASAP 2020 software.

3.3 Synthesis of NU-1000 ligand, 1,3,6,8-tetrakis(*p*-benzoic acid)pyrene (H_4TBAPy)

The synthesis of NU-1000 ligand, 1,3,6,8-tetrakis(p-benzoic acid)pyrene (H_4TBAPy) was adapted from a two-step procedure reported by Mondloch *et al.*.[43] as shown in Figure 5 (first step) and 6 (second step) below.

Synthesis of 1,3,6,8-tetrakis(4-(methoxycarbonyl)phenyl)pyrene:

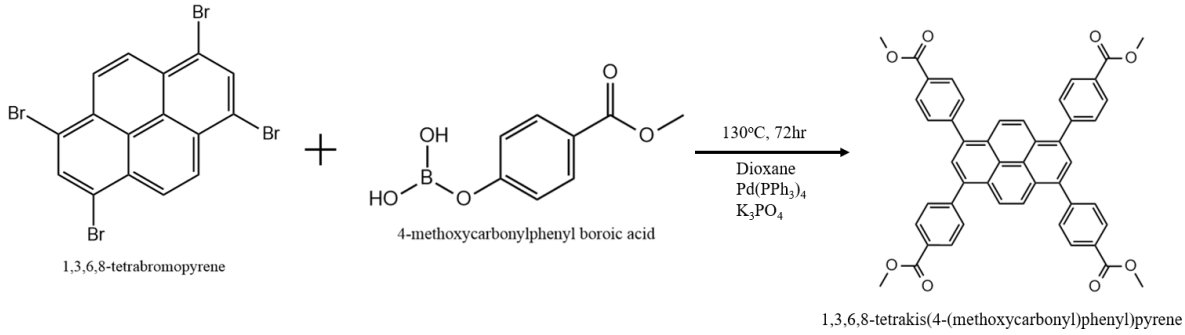

Figure 5. Synthetic scheme for 1,3,6,8-tetrakis(4-(methoxycarbonyl)phenyl)pyrene

In glove box, a mixture of (4-(methoxycarbonyl)phenyl)boronic acid (1.040 g, 5.80 mmol), 1,3,6,8-tetrabromopyrene (0.500 g, 0.97 mmol), potassium tribasic phosphate (1.100 g, 5.30 mmol), and tetrakis(triphenylphosphine) palladium(0) (0.030 g 0.026 mmol) were loaded into a 150 mL microwave vial (Biotage) and were mixed with 20 mL anhydrous 1,4-dioxane. The Biotage was then closed tightly with a cap, sealed with parafilm, and transferred outside of the glove box. This mixture was placed in an oil bath and stirred for 72 h at 130°C. After three days, the reaction mixture was transferred to a round bottom flask, and the solvent was evaporated to dryness by a rotary

evaporator. The solid residue was washed with water and then extracted with chloroform (repeated three times). The extract was dried by a rotary evaporator again and resulted in a bright yellow solid. This procedure gave 0.56 g of 1,3,6,8-tetrakis(4-(methoxycarbonyl)phenyl)pyrene (79% yield).

Synthesis of 1,3,6,8-tetrakis(*p*-benzoic acid)pyrene:

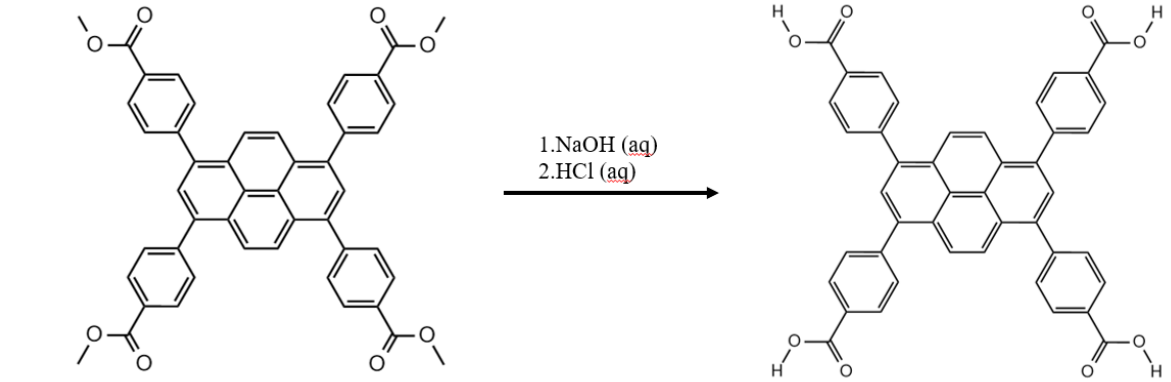

Figure 6. Synthetic scheme for 1,3,6,8-tetrakis(*p*-benzoic acid)pyrene

In a 250 mL round bottom flask containing 1,3,6,8-tetrakis(4-(methoxycarbonyl)phenyl)pyrene (0.56g, 0.57 mmol), a solution of NaOH (1.5g, 37.5 mmol), 50 mL THF, and 50 mL DI water was added, and the mixture was stirred under reflux overnight. On the next day, the mixture was evaporated by a rotary evaporated and 45 mL DI water was added to the round bottom flask and formed a clear yellow solution. The solution was then stirred for 2 hours at room temperature. After that, the solution was acidified to pH 1.0 by adding concentrated HCl. The yellow precipitate was then washed with DI water, collected by vacuum filtration, and dried in a vacuum oven overnight. The product was produced as a bright yellow solid (0.48 g, 90% yield). NMR was conducted to confirm the structure of 1,3,6,8-tetrakis(*p*-benzoic acid)pyrene (shown in Figure 7).

^1H NMR (DMSO-d_6): δ 7.856 (d, 8H), 8.087 (s, 2H), 8.160 (d, 8H), 8.211 (s, 4H), 13.119 (s, 4H).

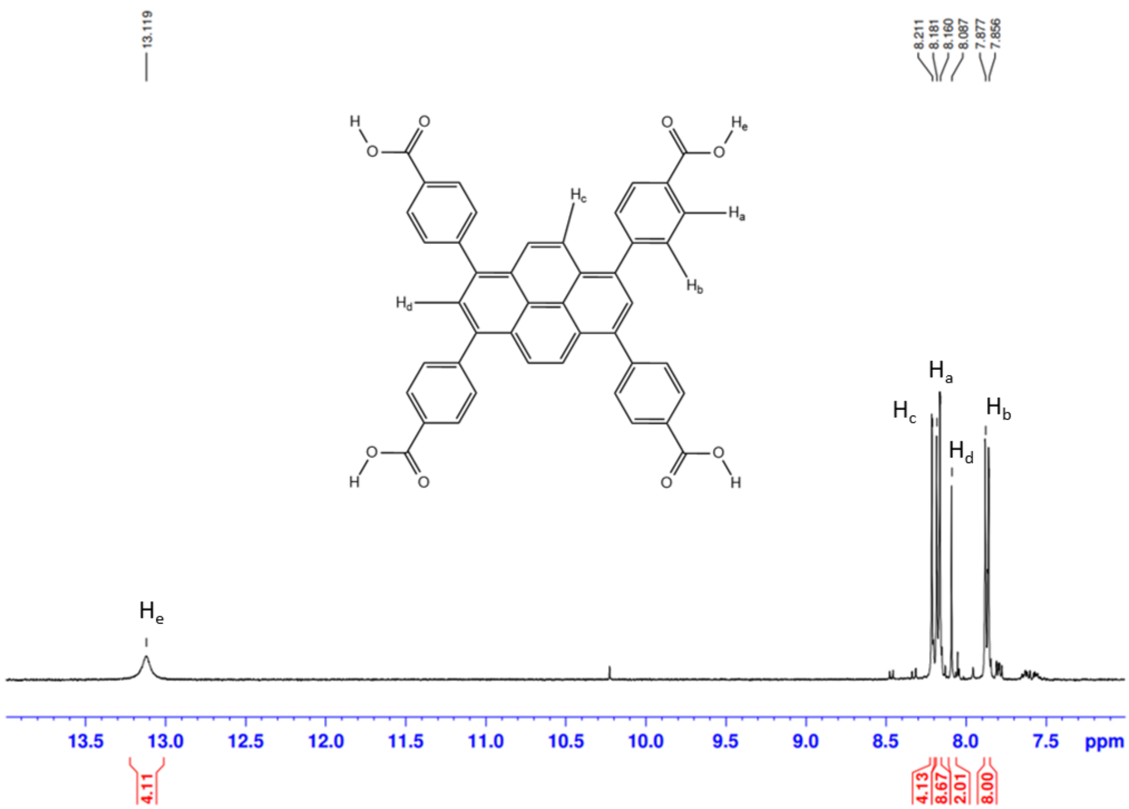

Figure 7. ^1H NMR spectrum for 1,3,6,8-tetrakis(*p*-benzoic acid)pyrene

3.4 Synthesis of modulator, 4-Azidomethyl-benzoic acid (4_AMBA)

The synthesis of 4-Azidomethyl-benzoic acid (4_AMBA) was adapted from the synthesis procedure reported by Foot *et al.*.[44] The synthesis scheme was showed in Figure 8 below.

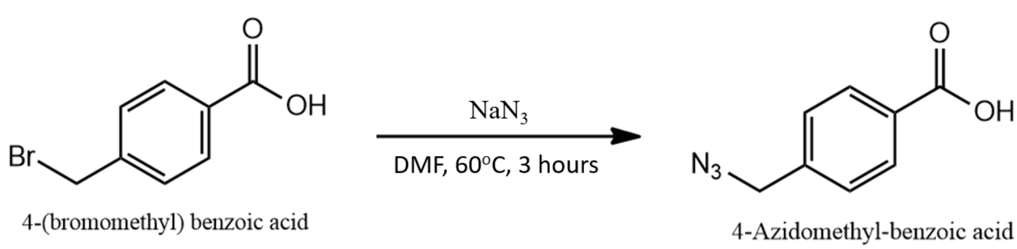

Figure 8. Synthesis scheme for 4-Azidomethyl-benzoic acid (4_AMBA)

In a 250 mL round bottom flask, 4-(bromomethyl) benzoic acid (0.645 g, 3 mmol) was dissolved in 10 mL DMF, and sodium azide (0.215 g, 3.3 mmol) was then added to the mixture. The reaction mixture was heated to 60° C for 3 hours. After that, the reaction mixture was cooled to room temperature. 50 mL DI water was then added to the cooled reaction mixture and a white precipitate formed. The resultant precipitate was filtered and dried by placing it in a vacuum oven overnight. The product was obtained as white solid (0.38 g, 70% yield). NMR was conducted to confirm the structure of 4_AMBA (shown in Figure 9). FT-IR was conducted to confirm the appearance of the azide group, and the signal of the azide functional group showed at 2,100 cm^{-1} (shown in Figure 10).

^{1}H NMR (DMSO-d_6): δ 4.569 (s, 2H), 7.479 (d, 2H), 7.959 (d, 2H)

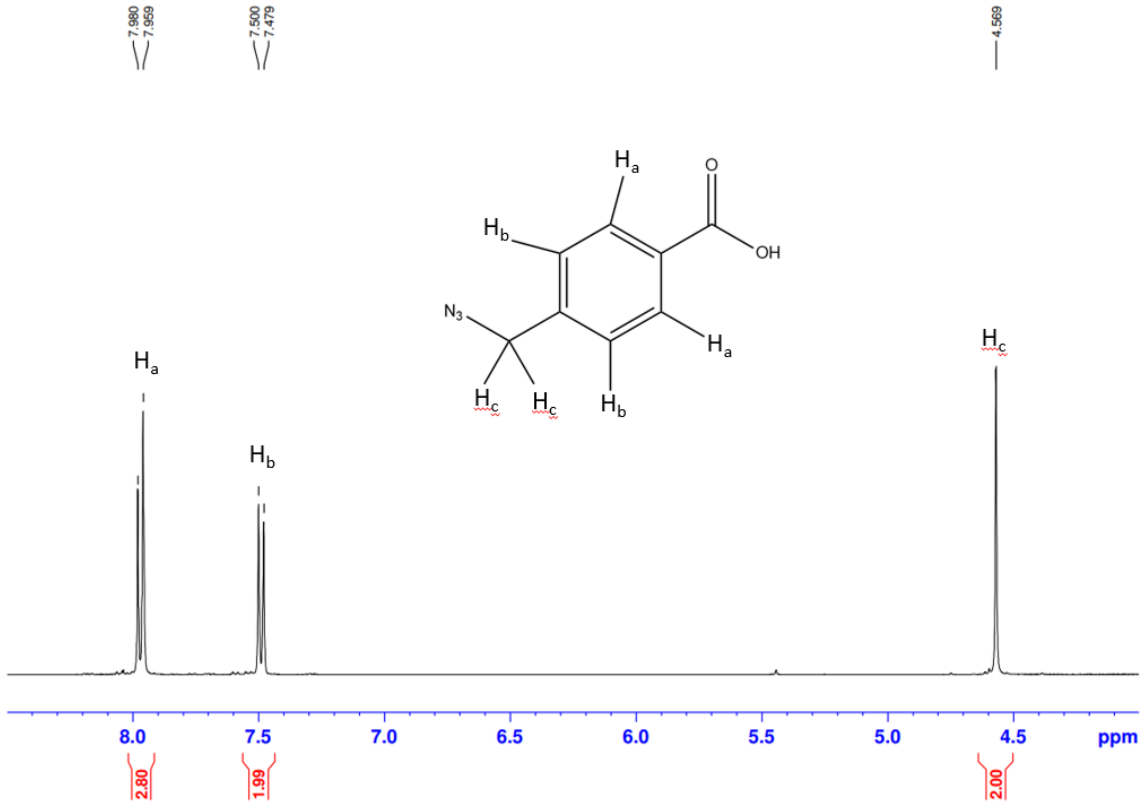

Figure 9. ^{1}H NMR spectrum for 4_AMBA

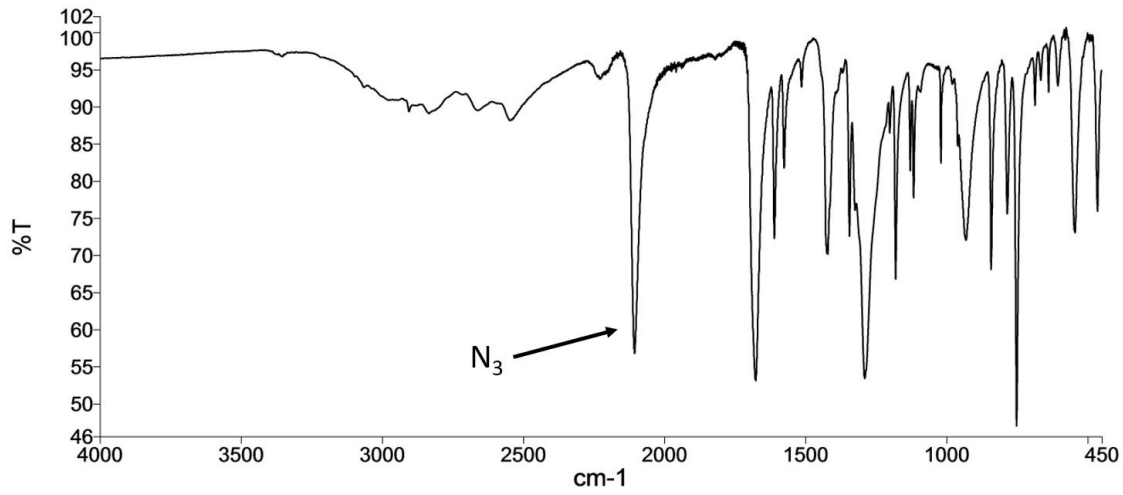

Figure 10. FT-IR spectra for 4_AMBA showing the presence of azide group

3.5 Synthesis of Polyethylene glycol 550-Propargyl (PEG550-Progargyl)

The synthesis of Polyethylene glycol 550-Propargyl (PEG550-Progargyl) was adapted from the literature written by Goswami *et al.*.[45] A synthesis scheme of PEG550-Progaryl is shown below in Figure 11.

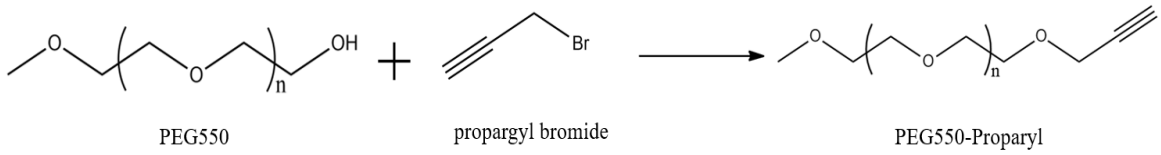

Figure 11. Synthesis Scheme for PEG550-Progaryl

The synthesis was performed under inert conditions. A mixture of NaH (0.230 g, 5.46 mmol) was dissolved in 20 mL anhydrous THF in a 150 mL microwave vial (Biotage). A solution of PEG550 (2 mL, 3.64 mmol) was mixed with 20 mL anhydrous THF and the solution was slowly added to the mixture in a glove box and was then stirred for 30 minutes at room temperature. After that, a solution of propargyl bromide (0.6 mL, 3.4 mmol) with 20 mL anhydrous THF was added to the mixture dropwise. The mixture was heated overnight at 60°C. On the next day, the reaction mixture was quenched with

100 mL 3% HCl and was then dried by using a rotary evaporator. The crude product was extracted with DCM and washed with brine (repeated three times). The organic layer was collected and was dried with Magnesium Sulfate to remove any water. The organic solvent was then removed by rotary evaporator and the product was collected as PEG550-Propargyl (1.760 g, 85% yield). NMR was performed to confirm the structure (shown in Figure 12).

^{1}H NMR (DMSO-d_6): δ 3.239 (s, 3H), 3.419-3.437 (m, 4H), 3.509-3.541 (m, 52H), 4.136 (d, 2H)

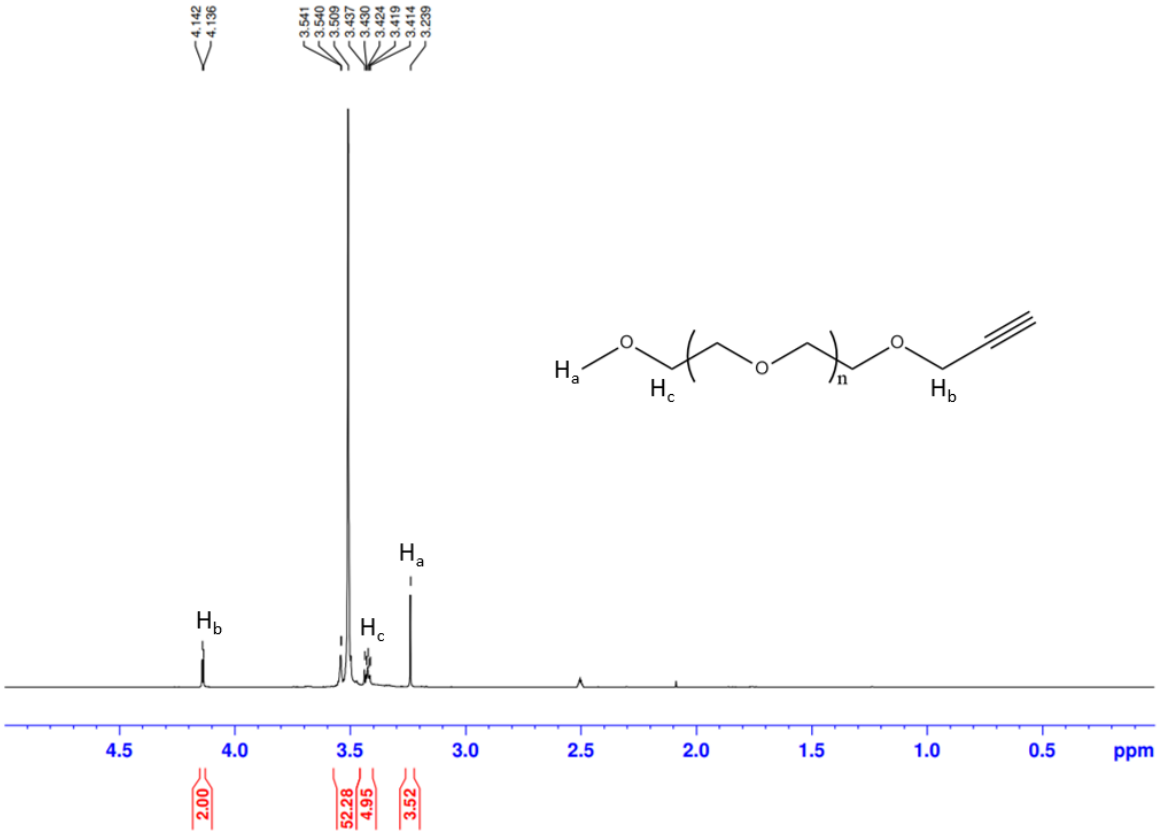

Figure 12. ^{1}H NMR spectrum for PEG550-Propargyl

3.6 Synthesis of UiO-66, MOF-808, NU-1000

UiO-66: The synthesis of UiO-66 was adapted from the literature published by Katz *et al.*.[34] In a 10-dram vial, $ZrCl_4$ (0.125 g, 0.54 mmol), 5 mL DMF, and 1 mL HCl

were loaded and sonicated for 20 minutes. After that, a solution of BDC (0.123 g, 0.75 mmol) and 10 mL DMF was added to the mixture. The mixture was continued to sonicate for an additional 20 minutes and was then transferred to the oven to be heated at 80^{o}C overnight. On the next day, the white precipitates that formed during the reaction were collected as UiO-66 by centrifugation (7830 rpm for 30 min). The product was then washed with 10 mL fresh DMF and 10 mL acetone (repeated three times) and collected by centrifugation. The white solid was dried in a vacuum oven overnight and was then characterized by PXRD and gas sorption.

MOF-808: The synthesis of MOF-808 was adapted from a reported procedure by Furukawa *et al.*.[46] In a 40 mL vial, $ZrOCl_2 \cdot 8H_2O$ (0.16 g, 0.5 mmol) and trimesic acid (0.11 g, 0.5 mmol) were dissolved in 20 mL DMF and 20 mL formic acid. The mixture was heated at 100^{o}C for seven days. The white precipitate was collected by centrifugation (7830 rpm for 30 min) and was then washed with 10 mL fresh DMF and 10 mL acetone (repeated three times). The product was dried in a vacuum oven overnight and collected as MOF-808. PXRD and gas sorption was performed to characterize MOF-808.

NU-1000: The synthesis of NU-1000 was adapted from Li *et al.*'s published literature.[36] Two solutions (Solution A and Solution B) were prepared prior to synthesis. Solution A: $ZrOCl_2 \cdot 8H_2O$ (970 mg, 3.00 mmol) and benzoic acid (16.0 g, 131 mmol) were dissolved in 80 mL DMF, and the mixture was heated at 100 ^{o}C for 1 hour. Solution B: 1,3,6,8-tetrakis(*p*-benzoic acid)pyrene (H4TBAPy) ligand (200 mg, 0.300 mmol) was dissolved in 80 mL DMF and the mixture was heated at 100 ^{o}C for 1 hour. Synthesis of NU-1000: In a 1.5-dram vial, 1 mL of Solution A, 1 mL of Solution B, and 20 μL of trifluoroacetic acid (0.26 mmol) were added resulting in a clear yellow solution.

(Repeated until Solution A or Solution B ran out). The vials were heated in a 100 ^{o}C oven for 1 hour or until a yellow suspension formed. After cooling down to room temperature, the vials were combined, and the precipitates were collected by centrifugation (7830 rpm for 30 min). The yellow solid was washed with 10 mL fresh DMF and acetone (repeated three times). HCl activation was performed by soaking approximately 50 mg of sample in 20 mL of DMF and 4 mL of 8 M HCl. The mixture was heated in an oven at 100 °C for 24 hours. The yellow product was collected by centrifugation (7830 rpm for 30 min) and was washed with 10 mL fresh DMF and acetone (repeated three times). The collected yellow product NU-1000 was dried in a vacuum oven overnight. PXRD and gas sorption was used to characterize NU-1000.

3.7 Synthesis of UiO-66-4_AMBA, MOF-808-4_AMBA, NU-1000-4_AMBA by SALI

The synthesis of UiO-66-4_AMBA, MOF-808-4_AMBA, and NU-1000-4_AMBA was accomplished by the Solvent Assisted Ligand Incorporation (SALI) method. The SALI procedure was adapted and adjusted based on the literature reported by Deria *et al*.[40]

UiO-66-4_AMBA: In a 10-dram vial, UiO-66 (100 mg, 0.060 mmol) was added to a solution of 4_AMBA (170 mg, 0.96 mmol) and 5 mL DMF. The mixture was sonicated for 20 minutes and was then heated at 60 ^{o}C overnight.

MOF-808-4_AMBA: In a 10-dram vial, MOF-808 (100 mg, 0.065 mmol) was added to a solution of 4_AMBA (184 mg, 1.04 mmol) and in 5 mL DMF. The mixture was sonicated for 20 minutes and heated at 60 ^{o}C overnight.

NU-1000-4_AMBA: In a 10-dram vial, NU-1000 (100 mg, 0.047 mmol) was added to a solution of 4_AMBA (132 mg, 0.750 mmol) and 5 mL DMF. The mixture was sonicated for 20 minutes and was then heated at 60 ^{o}C overnight.

After cooling down to room temperature, precipitates were collected by centrifugation (7830 rpm for 30 min) and were washed with 10 mL fresh DMF and acetone (repeated three times). Then, the products were dried in a vacuum oven overnight and were characterized by PXRD and gas sorption.

3.8 Synthesis of UiO-66-PEG, MOF-808-PEG, NU-1000-PEG by Copper-Catalyzed Azide–Alkyne Cycloaddition (CuAAC)

The PEGylation of MOFs procedure (CuAAC) was adapted from the literature reported by Lazaro *et al.*.[7] The synthesis was reacted under nitrogen, and DCM was previously degassed prior to the synthesis.

UiO-66-PEG: UiO-66-4_AMBA (100 mg, 0.060 mmol), CuI (2.5 mg, 0.027 mmol), DiPEA (152 µL, 0.027 mmol), acetic acid (46 µL, 0.027 mmol), and 20 mL degassed DCM were added to a 250 mL round bottom flask and stirred for 30 minutes. PEG550-Propargyl (598 µL, 1.100 mmol) was added dropwise, and the mixture was then allowed to react overnight at room temperature.

MOF-808-PEG: MOF-808-4_AMBA (100 mg, 0.065 mmol), CuI (4.0 mg, 0.042 mmol), DiPEA (243 µL, 0.042 mmol), acetic acid (74 µL, 0.042 mmol), and 20 mL degassed DCM were added to a 250 mL round bottom flask and stirred for 30 minutes. PEG550-Propargyl (957 µL, 2.56 mmol) was added dropwise, and the mixture was then allowed to react overnight at room temperature.

NU-1000-PEG: NU-1000-4_AMBA (100 mg, 0.047 mmol), CuI (2.8 mg, 0.030 mmol), DiPEA (172 µL, 0.030 mmol), acetic acid (52 µL, 0.030 mmol), and 20 mL degassed DCM were added to a 250 mL round bottom flask and stirred for 30 minutes. PEG550-Propargyl (957 µL, 2.56 mmol) was added dropwise, and the mixture was then allowed to react overnight at room temperature.

The products were collected by centrifugation (7830 rpm for 30 min) and were washed with 10 mL fresh DCM and MeOH (repeated three times). The products were then dried in a vacuum oven overnight. PXRD and gas sorption were used to characterize the products.

3.9 Calcein Loading on UiO-66-PEG, MOF-808-PEG, NU-1000-PEG

200 mg of UiO-66-PEG, MOF-808-PEG, or NU-1000-PEG were dispersed in 100 mL of a methanolic solution of calcein (10 mg/mL) by sonicating for 20 minutes and stirred at room temperature for 48 hours. The products were collected by centrifugation (4500 rpm, 20 min) and washed with fresh MeOH until the supernatant remained colorless (around 15 rounds). The products Cal@UiO-66-PEG, Cal@MOF-808-PEG, and Cal@NU-1000-PEG were dried in a vacuum oven overnight. PXRD and gas sorption were applied to characterize the PEGylated MOFs. FT-IR was also used to confirm the disappearance of the azide functional group (successful incorporation of PEG550-Propargyl onto 4_AMBA).

3.10 Calcein Release Experiment Set-up

The Calcein release experiments were monitored using a UV-Vis spectrophotometric analysis protocol similar to the degradation experiments. The

effect of PEGylated MOFs on calcein release was carried out in PBS at pH 7.4 and 5.5. The selectivity of PEGylation MOFs can be determined by these experiments. Dialysis tubing, an artificial semi-permeable tubing, was used in this experiment. The schematic experiment set-up is shown below in Figure 13.

10 mg calcein-loaded Zr-MOFs and PEGylated MOFs were placed in the pre-soaked dialysis tubing bags respectively. The filled dialysis bags were placed in the 100 mL PBS in a beaker. The experiments took four days. Around 5 mL samples were taken from the 100 mL PBS and were analyzed by UV-Vis to determine the amount of calcein that was diffused out from the dialysis bag during the experiments. The samples were poured back into the beaker after analysis. For the first five hours, samples were taken every half an hour. After that, samples were taken once per day.

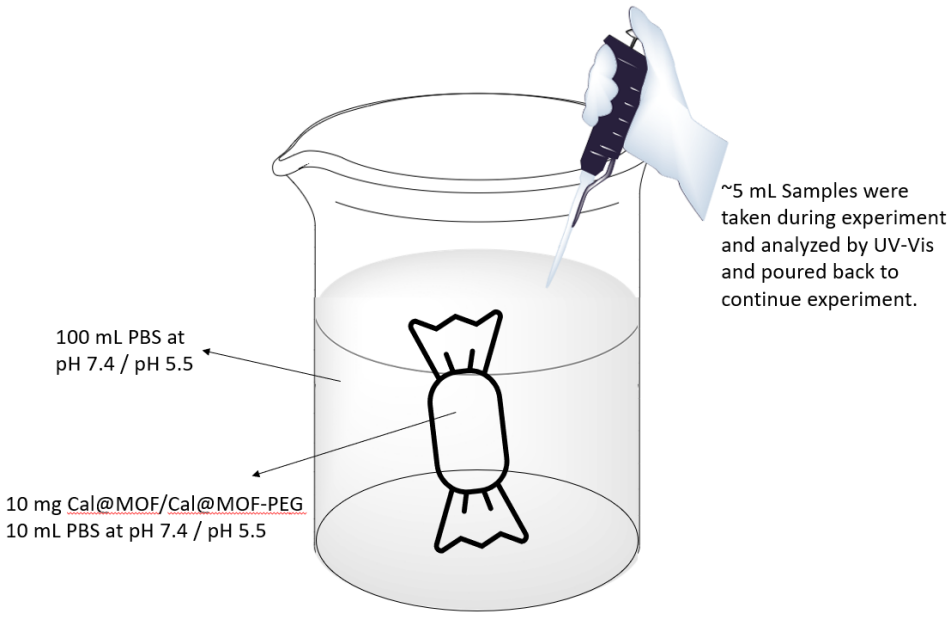

Figure 13. Schematic Experiment Set-up

A photo of the calcein-loaded unmodulated MOFs during the release experiment after 24 hours is shown below in Figure 14. The color change in the 100 mL PBS (originally colorless) indicated that calcein was released from the dialysis bag.

Figure 14. Experimental Set-Up

CHAPTER 4

Materials Characterizations and Calcein Calibration Curve

4.1 PXRD Characterizations

PXRD analysis of unmodified and modified UiO-66, MOF-808, and NU-1000 is shown below in Figures 15, 16, and 16, respectively. Analysis of the MOFs sample by PXRD confirmed their crystallinity. In particular, the well-defined PXRD patterns shown below confirmed that the PEGylated and 4_AMBA functionalized MOFs retained their crystallinity, indicating that the post-synthetic modifications did not affect the MOFs structures. More importantly, PXRD characterization confirmed that the unmodified and modified MOFs were stable structurally for further calcein loading.

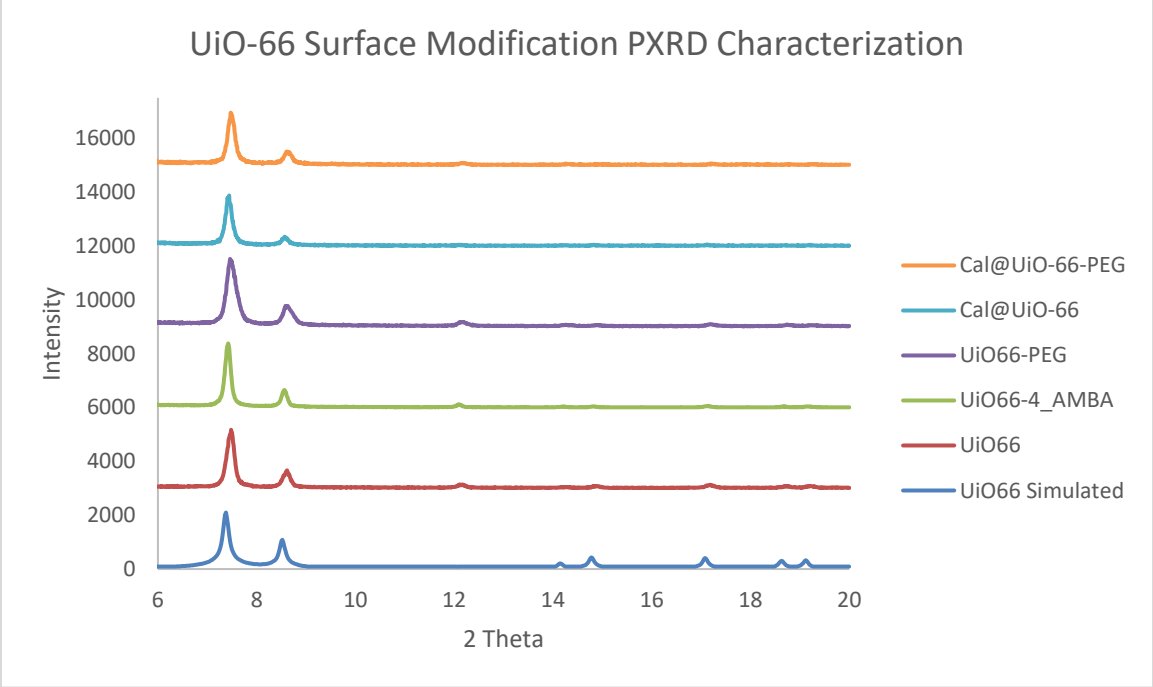

Figure 15. Stacked PXRD patterns of unmodified and modified UiO-66

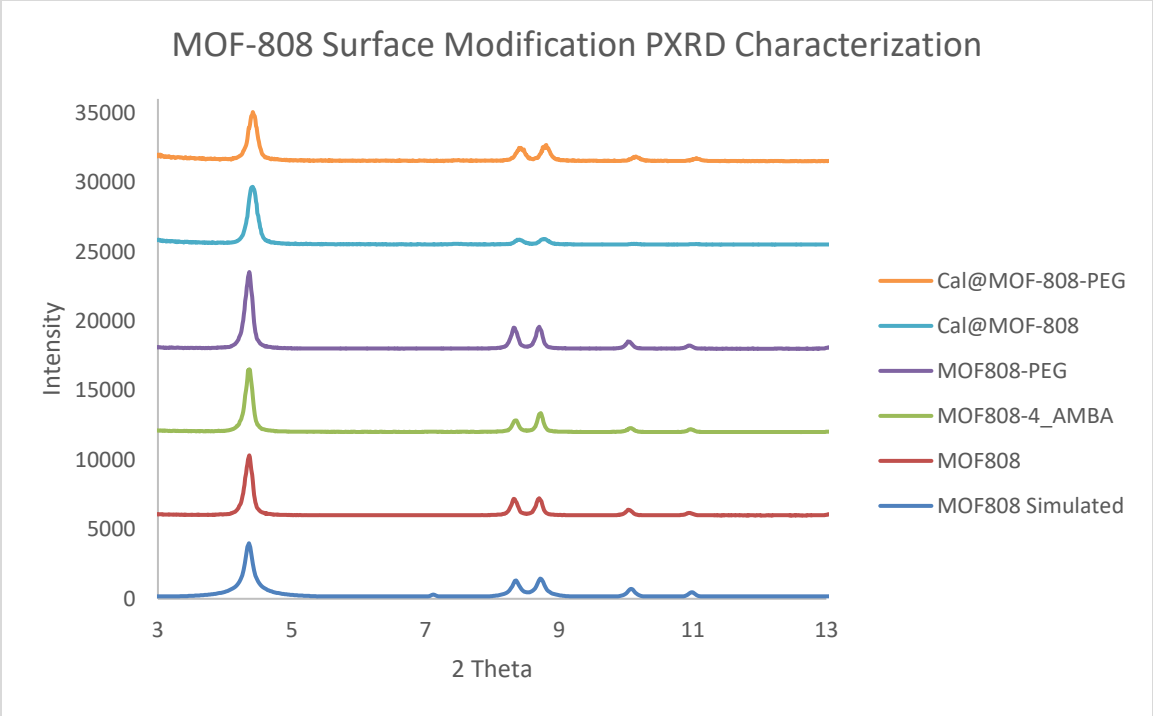

Figure 16. Stacked PXRD patterns of unmodified and modified MOF-808

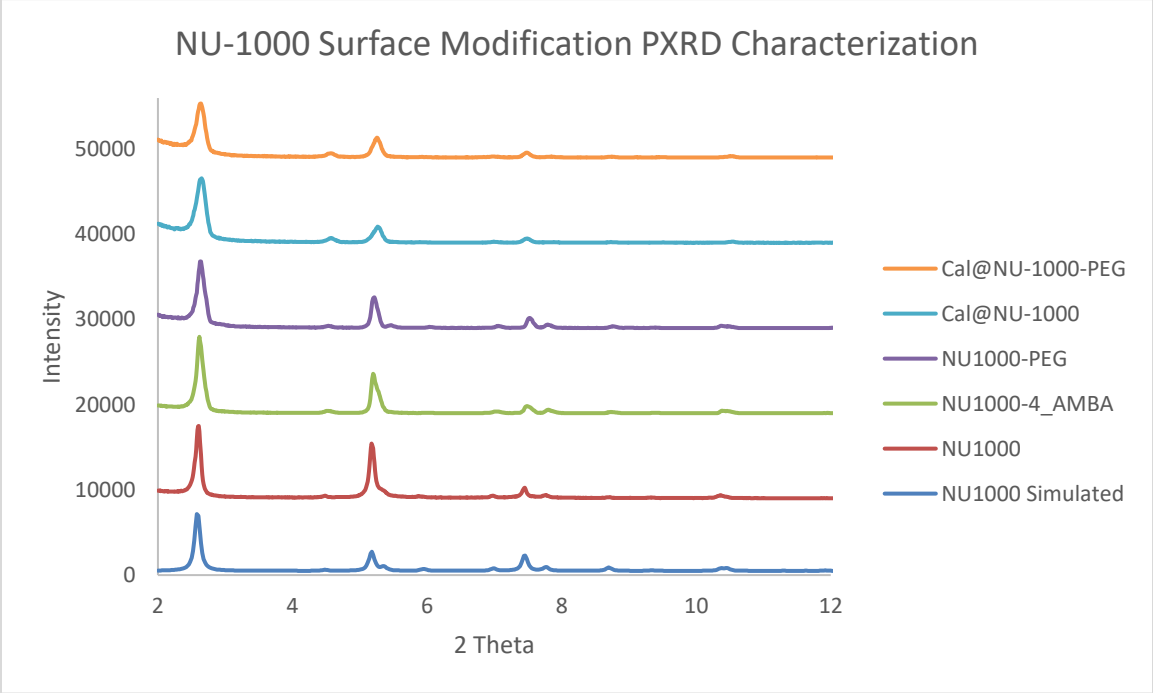

Figure 17. Stacked PXRD patterns of unmodified and modified NU-1000

4.2 FT-IR Characterizations

FT-IR spectra of 4_AMBA functionalized as well as PEGylated UiO-66, MOF-808, and NU-1000 are shown in Figures 18, 19, and 20, respectively. The 4_AMBA functionalized UiO-66, MOF-808, and NU-1000 showed an increase in signals associated with the azide group at 2100 cm^{-1}. The presence of azide peak on FT-IR spectra confirmed that the 4_AMBA was successfully incorporated onto the Zr clusters of MOFs and was ready for PEGylation. Furthermore, the FT-IR spectra of PEGylated UiO-66, MOF-808, and NU-1000 also showed the disappearance of signals for the azide group, which confirmed that the PEG550-Propargyl was successfully incorporated with 4_AMBA.

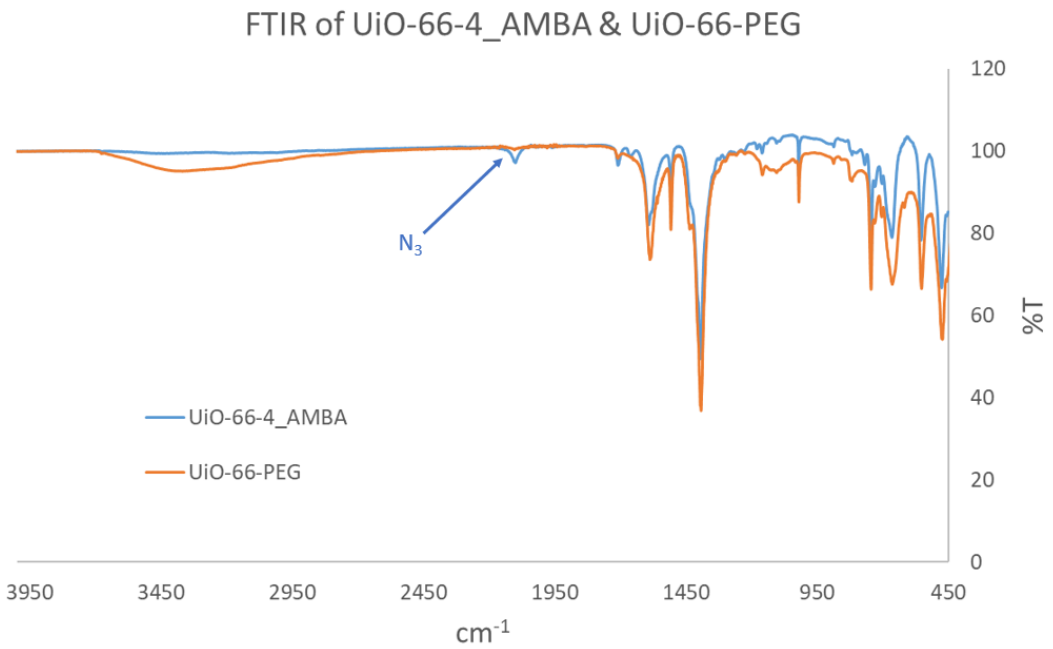

Figure 18. FT-IR spectra of UiO-66-4_AMBA and UiO-66-PEG

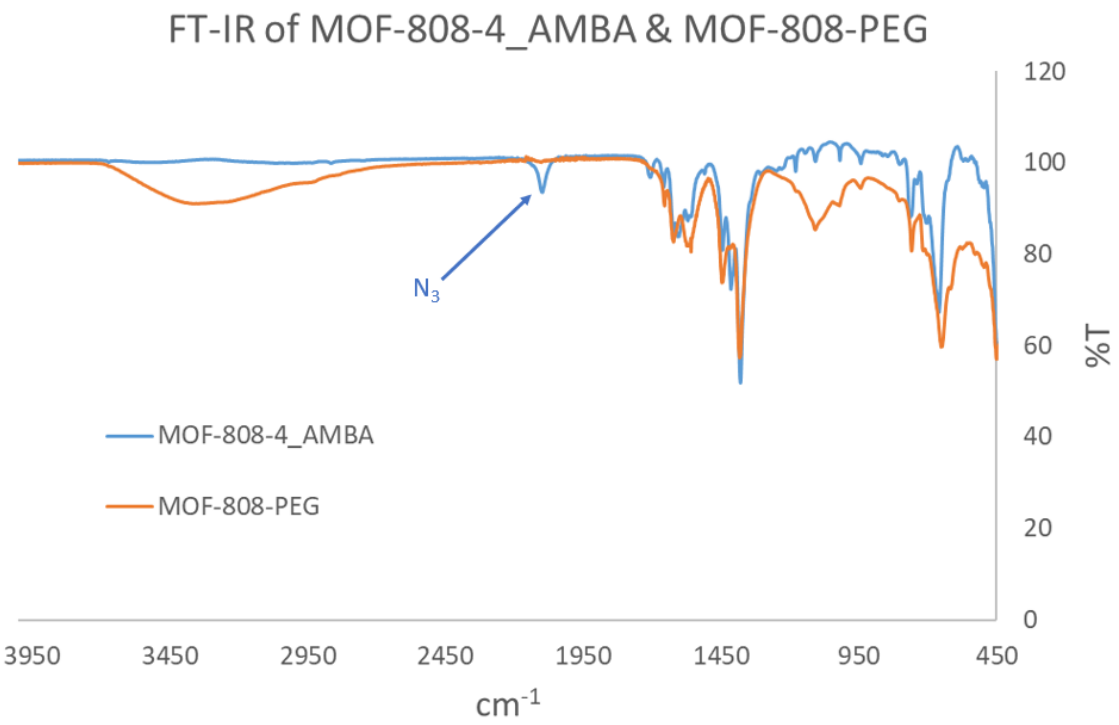

Figure 19. FT-IR spectra of MOF-808-4_AMBA and MOF-808-PEG

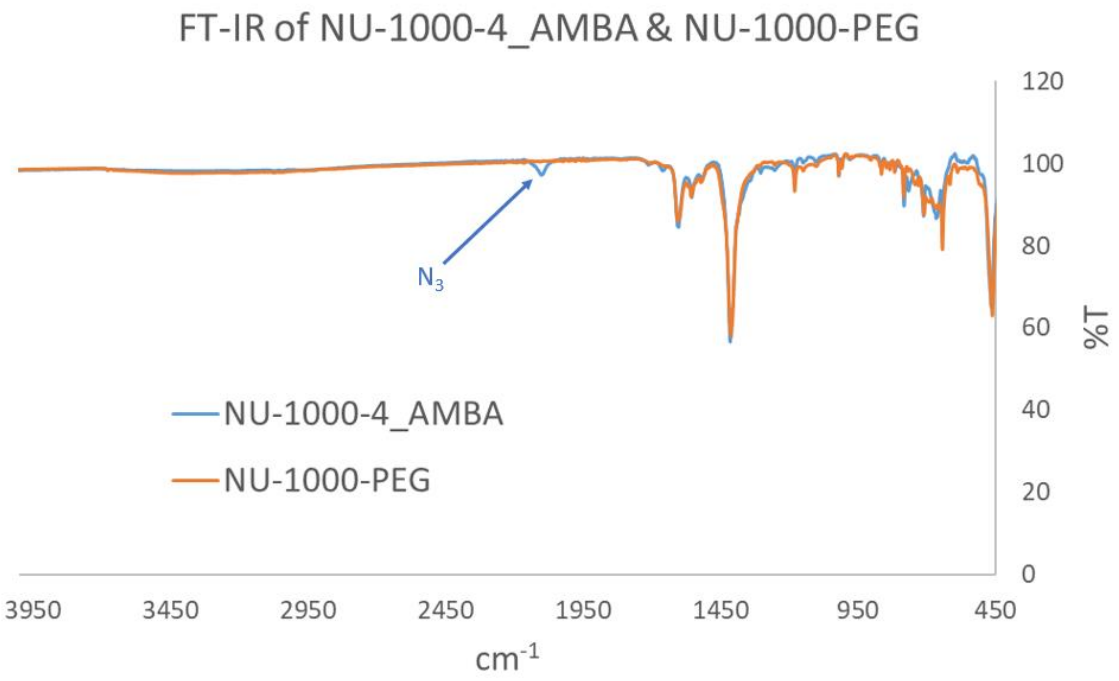

Figure 20. FT-IR spectra of NU-1000-4_AMBA and NU-1000-PEG

4.3 N_2 Adsorption Isotherms

Adsorption isotherms (N_2, 77 K) of unmodified, 4_AMBA functionalized, PEGylated, and calcein loaded UiO-66, MOF-808, and NU-1000 samples are shown in Figures 21, 22, and 23, respectively.

The N_2 adsorption isotherms showed an obvious decrease in surface area, which confirmed that the modulator/PEG/calcein were incorporated into the MOFs. Additionally, the analysis also suggested that the samples remained porous after calcein loading.

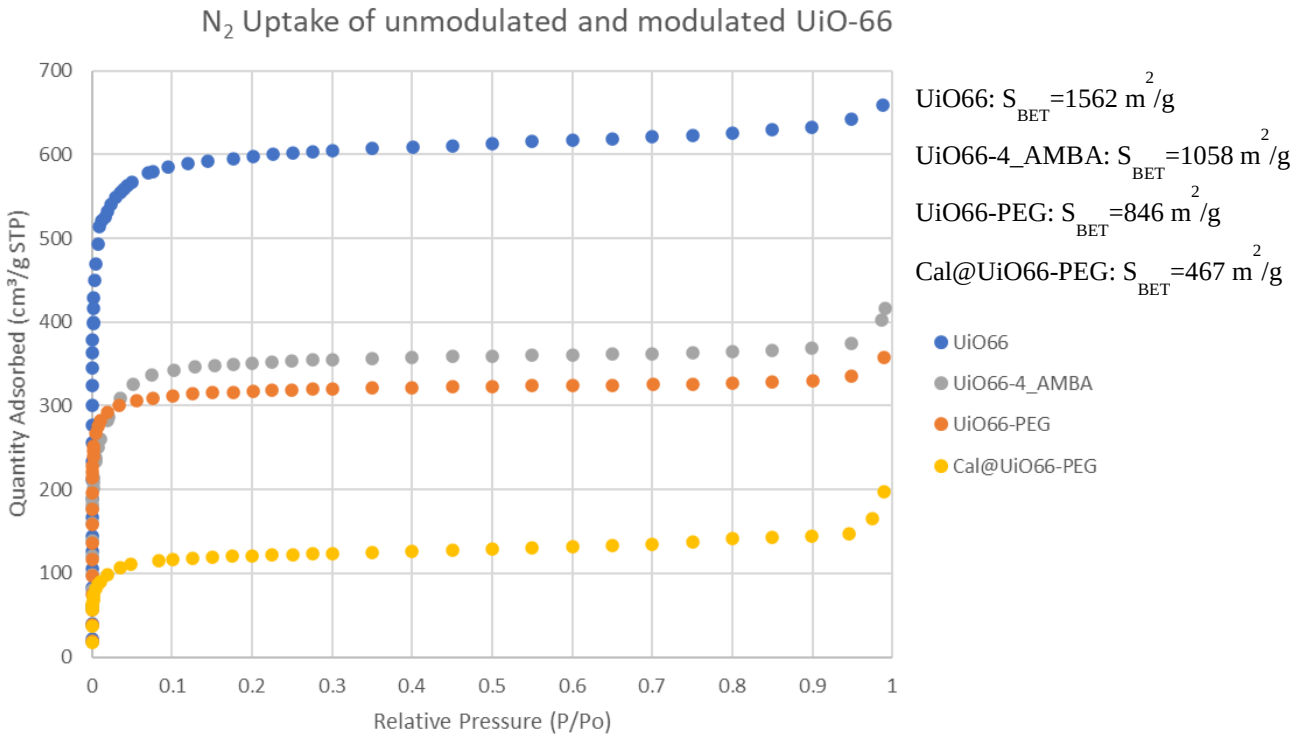

Figure 21. N_2 adsorption isotherms (77K) of unmodified, modified, and calcein loaded UiO-66

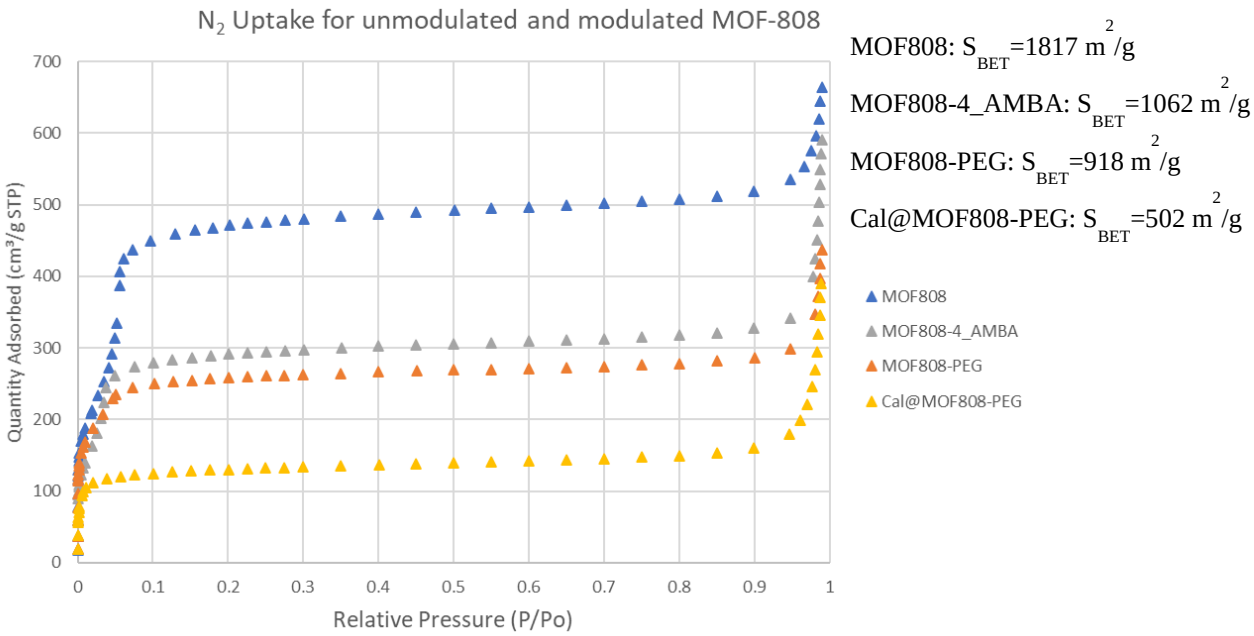

Figure 22. N_2 adsorption isotherms (77K) of unmodified, modified, and calcein loaded MOF-808

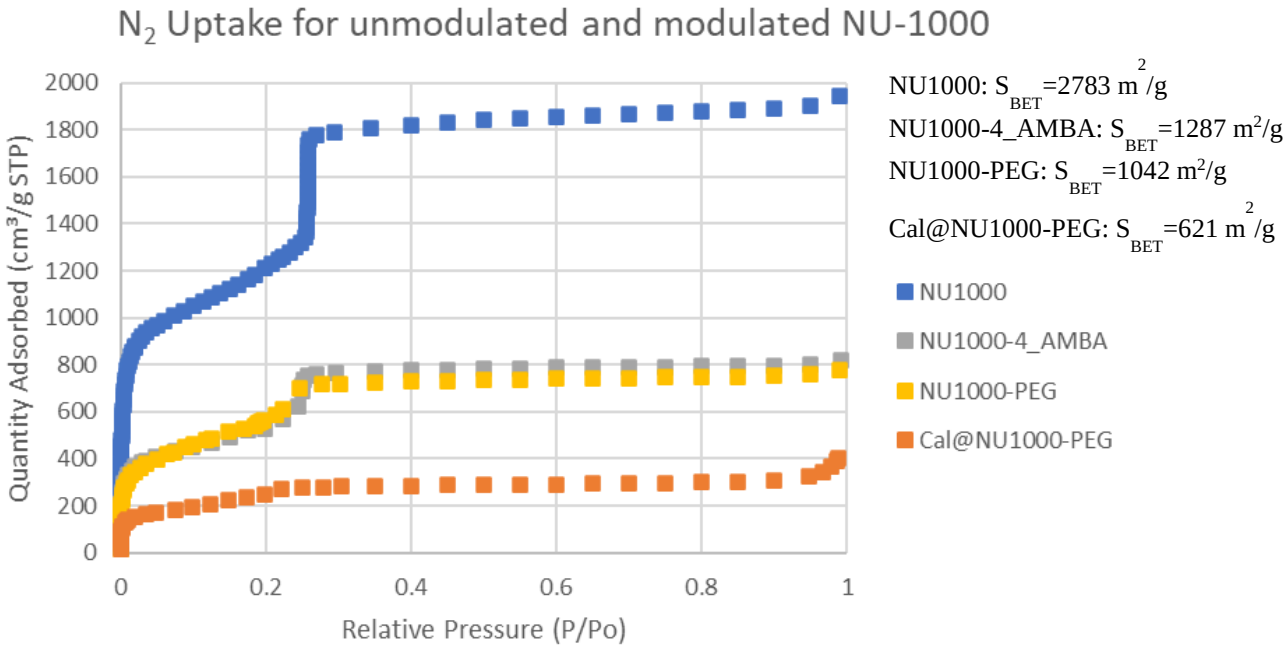

Figure 23. N_2 adsorption isotherms (77K) of unmodified, modified, and calcein loaded NU-1000

4.4 Determination of Calcein Loading

The calcein loading capacity of each MOF was determined by using UV-Vis spectrometry. 2 mg calcein loaded MOF was soaked in 40 mL KOH for three days to decompose the MOFs and release all the calcein contents in the basic solution. After three days, the samples were centrifuged to separate the solid and the supernatant. The remaining solid was observed to obtain a color of the original MOF which further confirmed that all the loaded calcein was released. The supernatant was collected and analyzed by UV-Vis to determine the percentage of calcein content in each MOF. A calcein calibration curve at 1M KOH (shown in Figure 24) was prepared to calculate the percentage of calcein content. The percentages of calcein content for each MOF were shown in the following table (shown in Table 1).

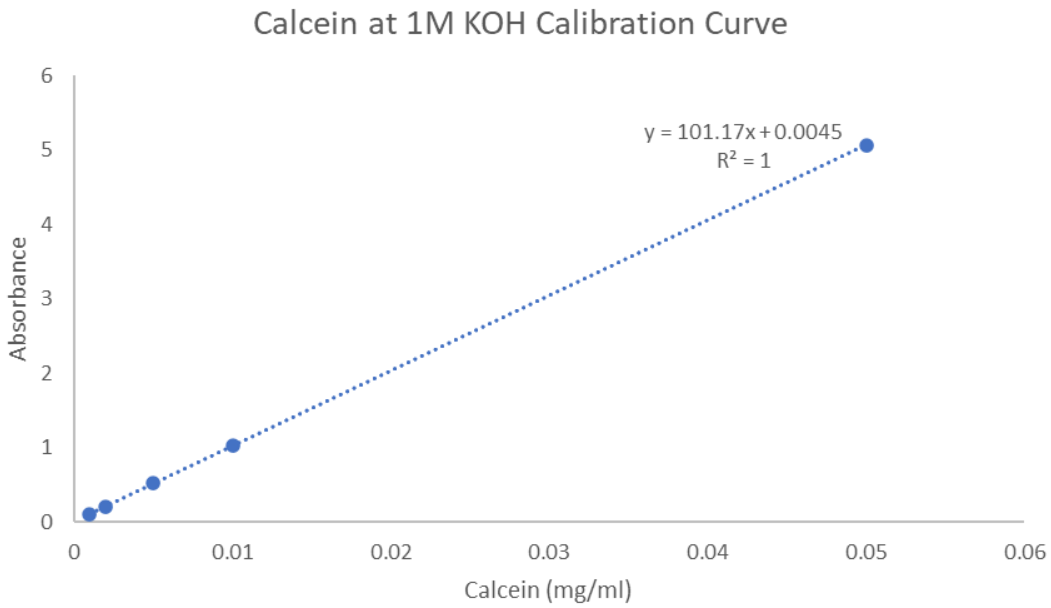

Figure 24. Calcein calibration curve at 1M KOH

4.5 Calcein Calibration Curve

To further investigate the calcein release kinetic from MOFs, the calibration curves of calcein in PBS at pH 7.4 and pH 5.5 were prepared before the experiments (shown below in Figures 25 and 26).

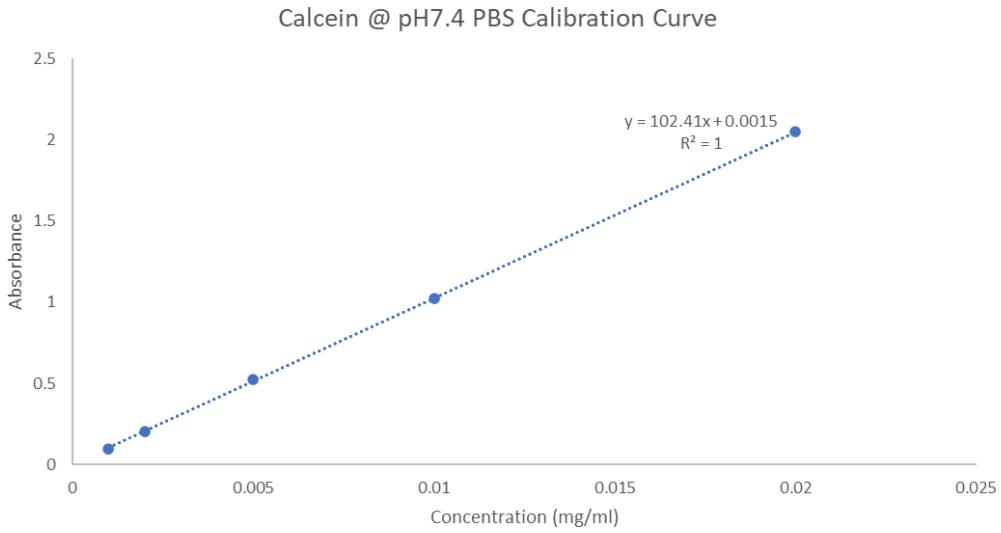

Figure 25. Calcein calibration curve at pH 7.4 PBS

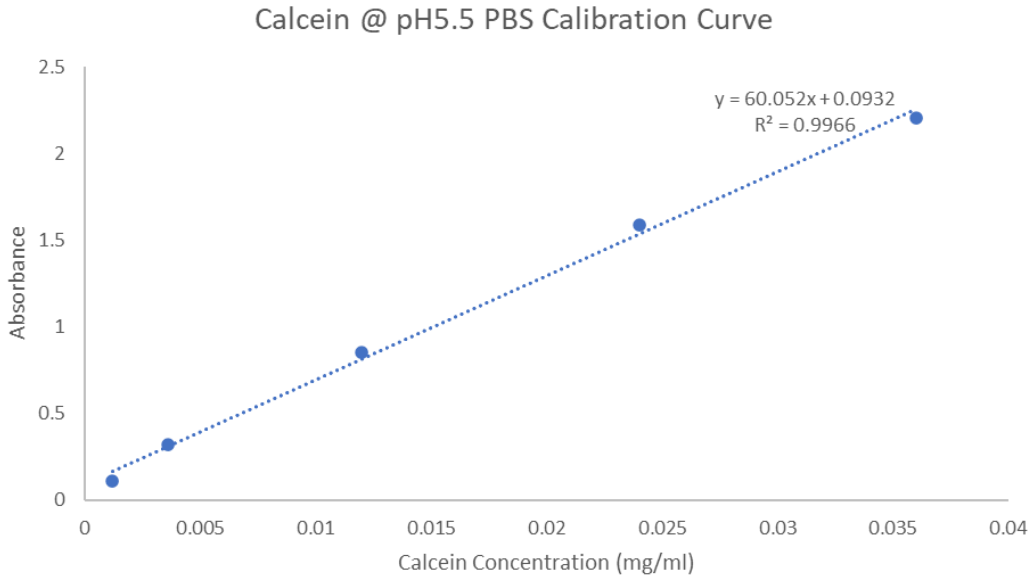

Figure 26. Calcein calibration curve at pH 5.5 PBS

CHAPTER 5

Results and Discussion

5.1 Calcein Loading

As shown in Table 1, the percentage of calcein content per calcein-loaded MOFs was determined by using UV-Vis and the calcein calibration curve at 1M KOH. The PEGylated MOFs were observed to have less calcein loaded compared to the unmodified MOFs. This could be explained by the surface modification on MOFs slightly blocking the route of calcein binding to the Zr cluster of MOFs and the smaller surface areas of the modified MOFs.

Table 1. Percentage of Calcein Content for each calcein loaded MOF

MOF	***% Calcein content***
Cal@UiO-66	73.12%
Cal@UiO-66-PEG	64.74%
Cal@MOF-808	73.13%
Cal@MOF-808-PEG	62.73%
Cal@NU-1000	71.46%
Cal@NU-1000-PEG	66.03%

5.2 Calcein Release

As shown in Figure 27, calcein release studies were performed for Cal@UiO-66 and Cal@UiO-66-PEG in pH 7.4 and pH 5.5 PBS. A significant difference in the release profiles was observed for the two pHs. Compared to physiological pH, both materials released calcein more rapidly under the acidic pH as expected. Under pH 7.4, the PEGylated UiO-66 exhibits a lower calcein release than the naked UiO-66. These results

suggest that the PEGylation can provide some protection for the MOFs from degradation under the physiological pH of healthy cells. This protection is not as significant under pH 5.5 as PEG can depolymerize under acidic pH, facilitating the pH-responsive properties of the PEGylated MOFs.

As a result, both Cal@UiO-66-PEG and Cal@UiO-66 under pH 5.5 showed relatively higher calcein release than pH 7.4. Due to the fact that the acidic PBS can lead to linker protonation, the MOFs were then decomposed rapidly at early time stages and released more quickly under pH 5.5. The unmodified UiO-66 was observed to have higher calcein release than PEGylated UiO-66 which suggests that the uncoated UiO-66 degraded faster without the protection from PEG.

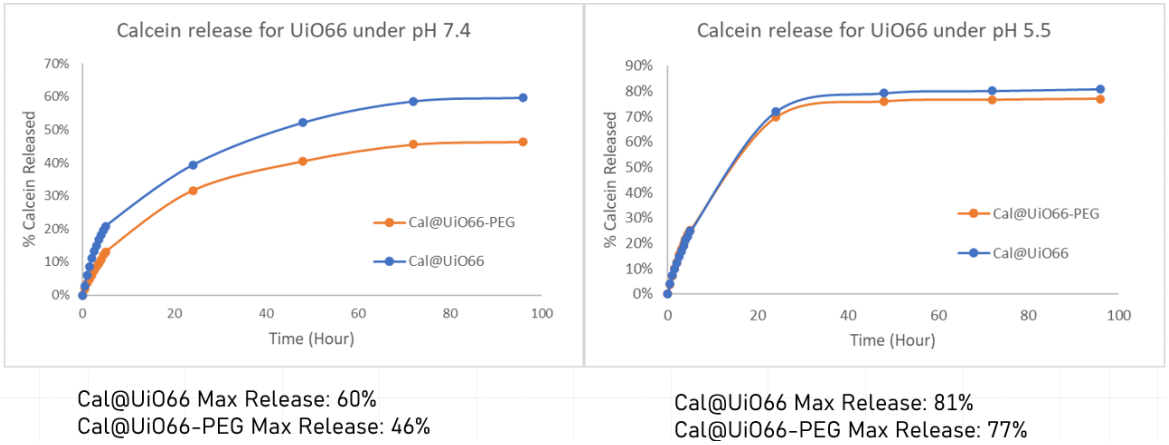

Cal@UiO66 Max Release: 60%
Cal@UiO66-PEG Max Release: 46%

Cal@UiO66 Max Release: 81%
Cal@UiO66-PEG Max Release: 77%

Figure 27. Calcein release kinetic for Cal@UiO-66 & Cal@UiO-66-PEG under pH 7.4 and pH 5.5

Likewise, MOF-808 and NU-1000 (shown in Figures 28 and 29) had shown similar characteristics in the calcein release experiments to UiO-66. All three Zr-MOFs had demonstrated that the PEGylation on MOFs efficiently protects the drug delivery carriers from degradation and facilitates the drug release to the targeted area (acidic conditions which correspond to tumor site environments).

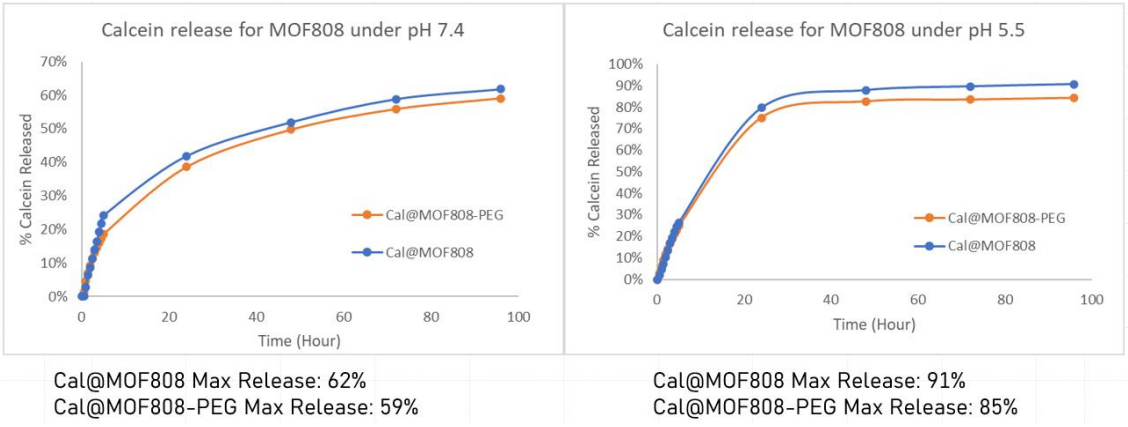

Cal@MOF808 Max Release: 62%
Cal@MOF808-PEG Max Release: 59%

Cal@MOF808 Max Release: 91%
Cal@MOF808-PEG Max Release: 85%

Figure 28. Calcein release kinetic for Cal@MOF-808 & Cal@MOF-808-PEG under pH 7.4 and pH 5.5

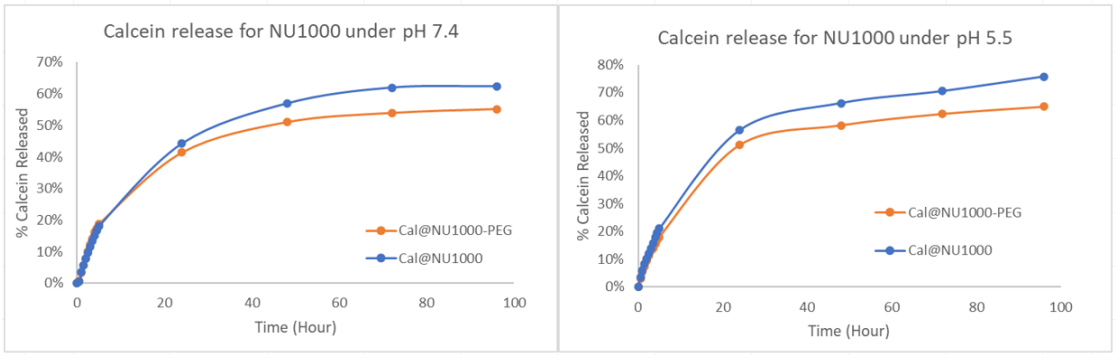

Cal@NU1000 Max Release: 62%
Cal@NU1000-PEG Max Release: 55%

Cal@NU1000 Max Release: 76%
Cal@NU1000-PEG Max Release: 65%

Figure 29. Calcein release kinetic for Cal@NU-1000 & Cal@NU-1000-PEG under pH 7.4 and pH 5.5

While all three Zr-MOFs behaved similarly in the experiments, UiO-66 had shown the best inhibition of drug release under pH 7.4 with the protection from PEG coating. Under pH 7.4, Cal@UiO-66-PEG only released 46% calcein while Cal@MOF-808-PEG and Cal@NU-1000-PEG released 59% and 55% respectively. Notably, compared to UiO-66 and MOF-808, NU-1000 showed a significantly lower release under pH 5.5. This could be explained by the fact that NU-1000 is more chemically stable than the other two MOFs. Therefore, the slower degradation NU-1000 leads to the lower release of calcein. The assumption mentioned earlier that a larger MOF aperture and larger MOF size could potentially increase the calcein uptake and facilitate higher release was not valid. Instead, the calcein release rate and amount is largely affected by the

chemical stability of the MOF. In our experiments, UiO-66, as the smallest MOF among all three selected Zr-MOFs, demonstrated the most efficient prevention of degradation under pH 7.4. That can be attributed to more accessible defect sites in UiO-66 for PEGylation, which helped to improve the protection of the MOF from degrading under pH 7.4.

CHAPTER 6

Conclusion and Future Work

6.1 Conclusion

Three Zr-MOFs, UiO-66, MOF-808, and NU-1000, were synthesized by incorporating zirconium clusters with different organic ligands to form MOFs with different pore sizes. Surface modifications using 4_AMBA and PEG550-Propargyl (PEGylation) on MOFs showed significant protection of MOFs from rapid degradation under extracellular pH conditions (pH 7.4). The PEGylated MOFs showed improved resistance to the attack from phosphates in the PBS, while the naked MOFs without the PEG coating exhibited a faster calcein release under pH 7.4. As the pH decreased (pH 5.5), the organic ligands of MOFs were more prone to protonation leading to MOF degradation and calcein release. Compared to pH 7.4, both naked MOFs and PEGylated MOFs showed increased calcein release under pH 5.5, while the PEGylated MOFs still showed a more sustained release over 100 hours. Both the pristine and PEGylated MOFs exhibited pH-responsive drug delivery behavior where more calcein was released under acidic conditions. However, compared to the pristine MOFs, the PEGylated MOFs showed lower calcein release under pH 7.4 (healthy cell environment) and more sustained calcein release under pH 5.5 (cancer cell environment). Our studies suggest that the PEGylation of MOFs can potentially further reduce the side effects of chemotherapy and realize target/sustained delivery to cancer cells.

6.2 Future Work

To further validate the release kinetics of the encapsulated calcein from the PEGylated MOFs and verify the stimuli-responsive behavior of the PEGylated MOFs, the

calcein release experiments will need to be repeated at least two more times. The general trends of the three replicates will be used to confirm the effects of PEGylation of MOFs on their pH-responsive drug delivery properties.

REFERENCES

1. Weinberg, R. A. How Cancer Arises. *Scientific American*. **1996**, 275(3), 62-70. https://www.jstor.org/stable/24993349

2. Seyfried, T. N.; Huysentruyt, L. C. On the origin of cancer metastasis. *Crit Rev Oncog.* **2013**, 18(1-2), 43-73. DOI: 10.1615/critrevoncog.v18.i1-2.40

3. *World Cancer Report 2020: Cancer Research for Cancer Prevention from Lyon: International Agency for Research on Cancer,* Wild, C. P., Weiderpass, E., Stewart, B. W., Eds., 2020. ISSN: 978-92-832-0447-3

4. *World Cancer Report 2014 from International Agency for Research on Cancer,* Steward, B. W., Wild, C. P., Eds., 2014. ISSN: 978-92-832-0429-9

5. Senapati, S.; Mahanta, A. K.; Kumar, S.; Maiti, P. Controlled drug delivery vehicles for cancer treatment and their performance. *Signal Transduction and Targeted Therapy*. **2018**, 3(7). DOI: 10.1038/s41392-017-0004-3

6. Wu, M.; Y, Y. Metal-Organic Framework (MOF)-Based Drug/Cargo Delivery and Cancer Therapy. *Adv Mater*. **2017**, 29(23). DOI: 10.1002/adma.201606134

7. Abánades Lázaro, I.; Haddad, S.; Sacca, S.; Orellana-Tavra, C.; Fairen-Jimenez, D.; Forgan, R. S. Selective Surface PEGylation of UiO-66 Nanoparticles for Enhanced Stability, Cell Uptake, and pH-Responsive Drug Delivery. *Chem*. 2017, 2(4), 561–578. DOI: 10.1016/j.chempr.2017.02.005

8. Utreja, P.; Jain, S.; Tiwary, A. K. Novel Drug Delivery Systems for Sustained and Targeted Delivery of Anticancer Drugs: Current Status and Future Prospects. *Current Drug Delivery*. **2010**, 7(2), 152-16. DOI: 10.2174/156720110791011783

9. Devi, V. K.; Jain, N.; Valli, K. S. Importance of Novel Drug Delivery Systems in Herbal Medicines. *Pharmacognosy Review*. **2010**, 4(7), 27-31. DOI: 10.4103/0973-7847.65322

10. Croy, S. R.; Kwon, G. S. Polymeric micelles for drug delivery. *Curr Pharm Des*. **2006**, 12(36), 4669-84. DOI: 10.2174/138161206779026245

11. Langner, M.; Kral, T. E. Liposome-based drug delivery systems. Liposome-based drug delivery systems. *Pol J Pharmacol*. **1999**, 51(3), 211-22. PMID: 10600035

12. Yadav, D.; Sandeep, K.; Pandey, D.; Dutta, R. K. Liposomes for Drug Delivery. *J Biotechnol Biomater*. **2017**, 7(4). DOI: 10.4172/2155-952X.1000276

13. Vallet-Regí, M.; Colilla, M.; Izquierdo-Barba, I.; Manzano, M. Mesoporous Silica Nanoparticles for Drug Delivery: Current Insights. *Molecules*. **2017**, 23(1), 47. DOI: 10.3390/molecules23010047

14. Desai, N.; Momin, M.; Khan, T.; Gharat, S.; Ningthoujam, R. S.; Omri, A. Metallic nanoparticles as drug delivery system for the treatment of cancer. *Expert Opinion on Drug Delivery*. **2021**, 18(9), 1261-1290. DOI: 10.1080/17425247.2021.1912008

15. Markopoulou, P.; Panagiotou, N.; Li, A.; Bueno-Perez, R.; Madden, D.; Buchanan, S.; Fairen-Jimenez, D.; Shiels, P. G.; Forgan, R. S. Identifying Differing Intracellular Cargo Release Mechanisms by Monitoring In Vitro Drug Delivery from MOFs in Real Time. *Cell reports physical science*. **2020**, 1(11), 100254. DOI: 10.1016/j.xcrp.2020.100254

16. Eddaoudi, M.; Moler, D. B.; Li, H.; Chen, B.; Reineke, T. M.; O'Keeffe, M.; Yaghi, O. M. Modular Chemistry: Secondary Building Units as a Basis for the Design of Highly Porous and Robust Metal-Organic Carboxylate Frameworks. *Acc. Chem. Res*. **2001**, 34(4), 319-330. DOI: 10.1021/ar000034b

17. Furukawa, H.; Go, Y. B.; Ko, N.; Park, Y. K.; Uribe-Romo, F. J.; Kim, J.; O'Keeffe, M.; Yaghi, O. M. Isoreticular Expansion of Metal–Organic Frameworks with Triangular and Square Building Units and the Lowest Calculated Density for Porous Crystals. *Inorg. Chem*. **2011**, 50(18), 9147–9152. DOI: 10.1021/ic201376t

18. McGuire, C.V.; Forgan, R.S. The surface chemistry of metal-organic frameworks. *Chem. Commun*. **2015**, 51, 5199–5217. DOI: 10.1039/c4cc04458d

19. Morris, R. E.; Wheatley, P. S.; Gas storage in nanoporous materials. *Angew Chem Int Ed Engl*. **2008**, 47(27), 4966-4981. DOI: 10.1002/anie.200703934

20. Li, J.; Sculley, J.; Zhou, H. Metal–Organic Frameworks for Separations. *Chem. Rev*. **2012**, 112(2), 869–932. DOI: 10.1021/cr200190s

21. Isaeva, V. I.; Kustov, L. M. The application of metal-organic frameworks in catalysis (Review). *Pet. Chem*. 2010, 50, 167–180. DOI: 10.1134/S0965544110030011

22. Abánades Lázaro, I.; Ross, S. F. Application of zirconium MOFs in drug delivery and biomedicine. *Coordination Chemistry Reviews*. **2019**, 380, 230-259. DOI: 10.1016/j.ccr.2018.09.009

23. Zhao, X.; Liu, S.; Hu, C.; Liu, Y.; Pang, M.; Lin, J. Controllable synthesis of monodispersed NU-1000 drug carrier for chemotherapy. *ACS Appl. Bio Mater*. **2019**, 2(10), 4436-4441. DOI: 10.1021/acsabm.9b00621

24. Zheng, H.; Zeng, Y.; Chen, J.; Lin, R.; Zhuang, W.; Cao, R.; Lin, Z. Zr-Based Metal−Organic Frameworks with Intrinsic Peroxidase-Like Activity for Ultradeep

Oxidative Desulfurization: Mechanism of H_2O_2 Decomposition. *Inorganic Chemistry*. **2019**, 58(10), 6983-6992. DOI: 10.1021/acs.inorgchem.9b00604

25. Abuchowski, A.; McCoy, J. R.; Palczuk, N.C.; Van Es, T.; Davis, F.F. Effect of covalent attachment of polyethylene glycol on immunogenicity and circulating life of bovine liver catalase. *J Biol Chem*. **1977**, 252(11), 3582-3586. PMID: 16907

26. Weissig, V.; Pettinger, T. K.; Murdock, N. Nanopharmaceuticals (part 1): products on the market. *Int J Nanomedicine*. **2014**, 9, 4357-4373. DOI:10.2147/IJN.S46900

27. Suk, J.S.; Xu, Q.; Kim, N.; Hanes, J.; Ensign, L. M. PEGylation as a strategy for improving nanoparticle-based drug and gene delivery. *Adv Drug Deliv Rev*. **2016**, 99(Pt A), 28-51. DOI:10.1016/j.addr.2015.09.012

28. Shi, L.; Zhang, J.; Zhao, M.; Tang, S.; Cheng, X.; Zhang, W.; Li, W.; Liu, X.; Peng, H.; Wang, Q. Effects of polyethylene glycol on the surface of nanoparticles for targeted drug delivery. *Nanoscale*. **2021**, 13, 10748-10764. DOI: 10.1039/d1nr02065j

29. Fam, S. Y.; Chee, C. F.; Yong, C. Y.; Ho, K. L.; Mariatulqabtiah, A. R.; Tan, W. S. Stealth Coating of Nanoparticles in Drug-Delivery Systems. *Nanomaterials*. **2020**, 10(4), 787. DOI: 10.3390/nano10040787

30. Hoang Thi, T.T.; Pilkington, E. H.; Nguyen, D. H.; Lee, J. S.; Park, K. D.; Truong, N. P. The Importance of Poly(ethylene glycol) Alternatives for Overcoming PEG Immunogenicity in Drug Delivery and Bioconjugation. *Polymers.* **2020**, 12(2), 298. DOI: 10.3390/polym12020298

31. Bunzen, H. Chemical Stability of Metal-organic Frameworks for Applications in Drug Delivery. *ChemNanoMat*. **2021**, 7(9), 998-1007. DOI: 10.1002/cnma.202100226

32. Arifin, D. R.; Palmer, A. F. Physical Properties and Stability Mechanisms of Poly(Ethylene Glycol) Conjugated Liposome Encapsulated Hemoglobin Dispersions. *Artificial Cells, Blood Substitutes, and Biotechnology*. **2009**, 33(2), 137-162. DOI: 10.1081/BIO-200055880

33. Orellana-Tavra, C.; Marshall, R. J.; Baxter, E. F.; Abánades Lázaro, I.; Tao, A.; Cheetham, A. K.; Forgan, R. S.; Fairen-Jimenez, D. Drug delivery and controlled release from biocompatible metal–organic frameworks using mechanical amorphization. *J. Mater. Chem. B*. **2016**, 4, 7697. DOI: DOI: 10.1039/c6tb02025a

34. Katz, M. J.; Brown, Z. J.; Colón, Y. J.; Siu, P. W.; Scheidt, K. A.; Snurr, R. Q.; Hupp, J. T.; Farha, O. K. A Facile Synthesis of UiO-66, UiO-67 and Their Derivatives. *Chem. Commun*. **2013**, 49 (82), 9449–9451. DOI: 10.1039/c3cc46105j

35. Ma, K.; Wasson, M. C.; Wang, X.; Zhang, X.; Idrees, K. B.; Chen, Z.; Wu, Y.; Lee, S.; Cao, R.; Chen, Y.; Yang, L.; Son, F. A.; Islamoglu, T.; Peterson, G. W.; Mahle, J. J.; Farha, O. K. Near-instantaneous catalytic hydrolysis of organophosphorus nerve agents with zirconium-based MOF/hydrogel composites. *Chem Catalysis*. **2021**, 1(3), 721-733. DOI: 10.1016/j.checat.2021.06.008

36. Li, P.; Klet, R. C.; Moon, S. Y.; Wang, T. C.; Deria, P.; Peters, A. W.; Klahr, B. M.; Park, H. J.; Al-Juaid, S. S.; Hupp, J. T.; Farha, O. K. Synthesis of Nanocrystals of Zr-Based Metal-Organic Frameworks with Csq-Net: Significant Enhancement in the Degradation of a Nerve Agent Simulant. *Chem. Commun*. **2015**, 51(54), 10925–10928. DOI: 10.1039/c5cc03398e.

37. Cavka, J. H.; Jakobsen, S.; Olsbye, U.; Guillou, N.; Lamberti, C.; Bordiga, S.; Lillerud, K. P. A New Zirconium Inorganic Building Brick Forming Metal Organic Frameworks with Exceptional Stability. *JACS Communications.* **2008**, 130(42), 13850–13851. DOI:10.1021/ja8057953

38. Dong, H.; Yang, G.; Zhang, X.; Meng, X.; Sheng, J.; Sun, X.; Feng, Y.; Zhang, F. Folic Acid Functionalized Zirconium-Based Metal–Organic Frameworks as Drug Carriers for Active Tumor-Targeted Drug Delivery. *Chemistry – A European Journal.* **2018**, 24(64), 17148-17154. DOI: 10.1002/chem.201804153

39. Deria, P.; Chung, Y. G.; Snurr, R. Q.; Hupp, J. T.; Farha, O. K. Water stabilization of Zr_6-based metal–organic frameworks via solvent-assisted ligand incorporation. *Chem. Sci*. **2015**,6, 5172-5176. DOI: 10.1039/c5sc01784j

40. Derua, P.; Bury, W.; Hupp, J. T.; Farha, O. K. Versatile functionalization of the NU-1000 platform by solvent-assisted ligand incorporation. *Chem. Commun*. **2014**, 50, 1965-1968. DOI: 10.1039/c3cc48562e

41. Jankovič, D.; Virant, M.; Gazvoda, M. Copper-Catalyzed Azide−Alkyne Cycloaddition of Hydrazoic Acid Formed In Situ from Sodium Azide Affords 4-Monosubstituted-1,2,3-Triazoles. *The Journal of Organic Chemistry*. **2022**, 87(6), 4018-4028. DOI: 10.1021/acs.joc.1c02775

42. Orellana-Tavra, C.; Baxter, E. F.; Tian, T.; Bennett, T. D.; Slater, N. K. H.; Cheetham, A. K.; Fairen-Jimenez, D. Amorphous metal-organic frameworks for drug delivery. *Chem. Commun*. **2015**, 51, 13878-13881. DOI: 10.1039/x0xx00000x

43. Mondloch, J. E.; Bury, W.; Fairen-Jimenez, D.; Kwon, S.; Demarco, E. J.; Weston, M. H.; 38 Sarjeant, A. A.; Nguyen, S. T.; Stair, P. C.; Snurr, R. Q.; Farha, O. K.; Hupp, J. T. Vapor-Phase Metalation by Atomic Layer Deposition in a Metal-Organic Framework. *J. Am. Chem. Soc*. **2013**, 135 (28), 10294–10297. DOI: 10.1021/ja4050828

44. Foot, J. S.; Lui, F. E.; Kluger, R. Hemoglobin Bis-Tetramers via Cooperative Azide–Alkyne Coupling. *Chem. Commun*. **2009**, 47, 7315. DOI: 10.1039/b918860f

45. Goswami, L. N.; Houston, Z. H.; Sarma, S. J.; Jalisatgi, S. S.; Hawthorne, M. F. Efficient synthesis of diverse heterobifunctionalized clickable oligo(ethylene glycol) linkers: potential applications in bioconjugation and targeted drug delivery. *Org. Biomol. Chem*. **2013**, 11, 1116. DOI: 10.1039/c2ob26968f

46. Furukawa, H.; Gandara, F.; Zhang, Y.; Jiang, J.; Queen, W. L.; Hudson, M. R.; Yaghi, O. M. Water Adsorption in Porous Metal–Organic Frameworks and Related Materials. *J. Am. Chem. Soc*. **2014**, 136 (11), 4369–4381. DOI: 10.1021/ja500330a.